UiT
THE ARCTIC
UNIVERSITY
OF NORWAY

Faculty of Science and Technology
Department of Physics and Technology

On Trapped Particle Dynamics in Rotating Frames

Aurora Driveklepp Helgeland

FYS-3931 Master's Thesis in Space Physics 30 SP
July 2021

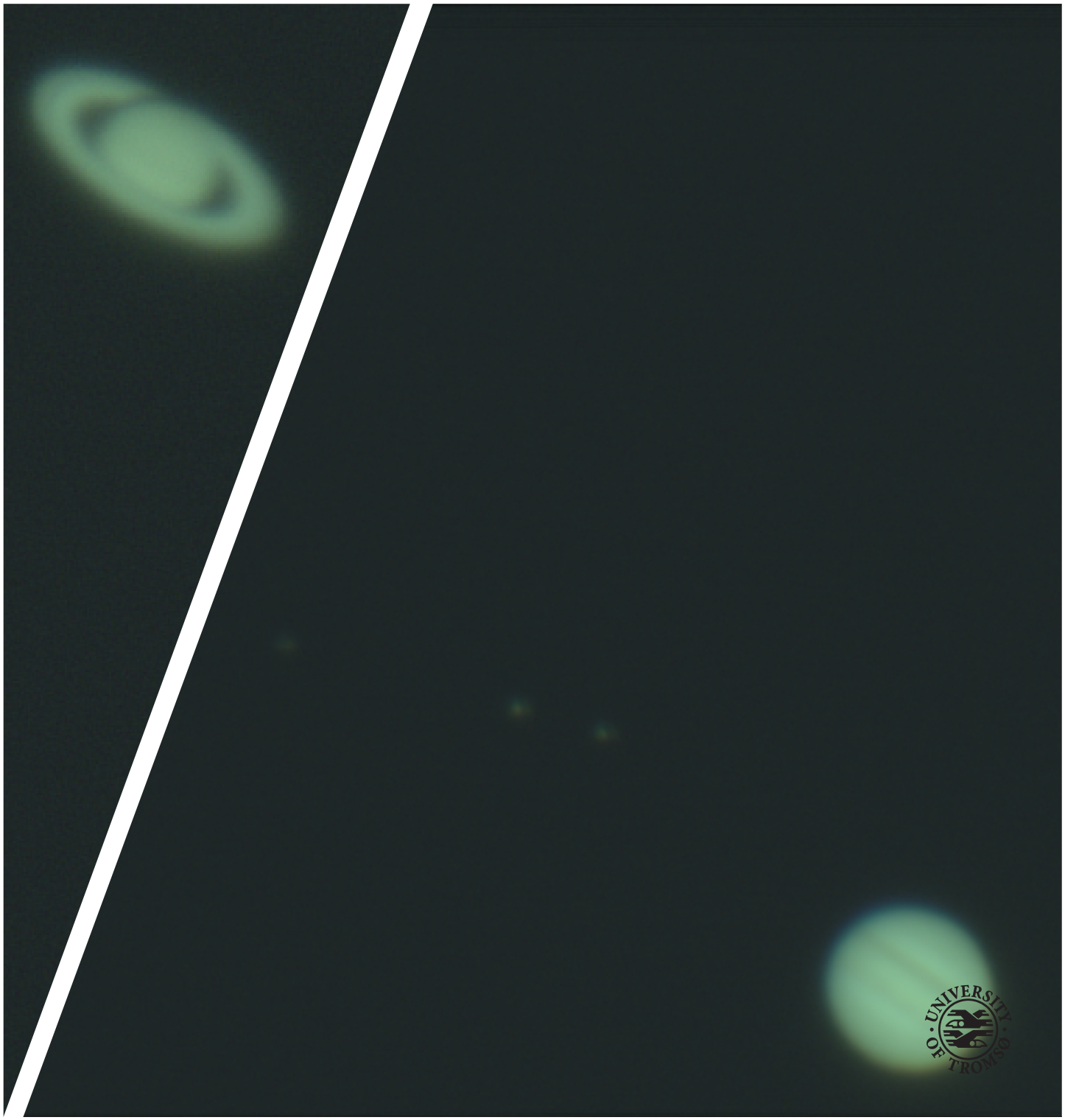

During the night of 23 October 2019, a series of images of Jupiter and Saturn were obtained at an observing site on Mauna Loa, Hawai´i. The front page image shows Saturn to the left, and Jupiter to the right, together with three of its Galilean moons; Io, Europa, and Ganymede. My team and I were able to capture these images by a Celestron scope with a QHY 178c camera system, with an exposure time varying between 30 and 180 seconds. We used the RegiStax system to stack frames from the short video exposures. Unfortunately, the wind began to pick up throughout the night, and we decreased the exposure times to accommodate for any movement it had on the videos. The final image results were not too promising, and since we were unable to see any main features of the planets, future observations should be done on a clearer night. The observation was fun, though very cold, and I am grateful for have gained some insight and experience in observational astronomy during my time abroad in Hilo.

Abstract

The rapid rotation of Jupiter and Saturn, combined with internal source of plasma provided by their moons Io and Enceladus respectively, creates a magnetodisk structure of the planetary magnetic field. The magnetodisk looks like a stretched dipole magnetic field in the equatorial region, where centrifugal force is largest. The centrifugal force, originating in the rotating frame, is known to have large contribution to the magnetodisk structure in the Jovian and Kronian magnetospheres. In order to investigate deviations in the dynamics of charged particles trapped in a magnetodisk compared to a pure dipole magnetic field, this thesis studies how centrifugal force influences a trapped particle's bounce motion as described by the so-called guiding centre approximation.

Here a model characterising a trapped particle's bounce period in a rotating frame of reference is presented. It is evident that conservation of energy and conservation of first adiabatic invariant put constraints on the particle motion along the field line. The β_{eq} parameter is a boundary condition to the model that determines the rate of change between kinetic and potential energy along the field line, and describes to which degree the system is affected by rotation. The bounce period is larger than in a non-rotating frame when inverse parallel velocity component increases faster than mirror point latitude decreases, and shorter for the opposite case. How these components change in relation to each other varies as a function of β_{eq}. Small values of β_{eq} results in longer bounce periods for particles with small equatorial pitch angles, and shorter bounce periods for particles with large equatorial pitch angles. An effect of rotation when β_{eq} increases is that also particles with small pitch angles are confined towards equator, bouncing with shorter bounce periods compared to a non-rotating frame. The β_{eq} parameter, describing the ratio of centrifugal potential energy to kinetic energy at equator, is thus a prerequisite for the particle dynamics along the field line in a rotating frame.

Acknowledgements

Thanks to my supervisor Patrick Guio for guiding me through this project, for your input, the academic insight and the discussions. Thanks to Björn Guvstavsson for the open door and that you always answer my quick questions thoroughly. Thanks for all the love and care in the Space Physics group. Thanks to those of you that have contributed in big and small discussions, in proof reading and otherwise been supportive in life, the universe and everything.

Contents

List of Figures

List of Tables

1

Introduction

When the kinetic energy of plasma particles in the Sun's corona reaches a certain value, they escape the Sun's gravitational field and flows out into space as solar wind. The interaction of solar wind and a planet's magnetic field creates a magnetosphere; a region of plasma surrounding the planet which is controlled by the magnetic field. Such planetary magnetospheres are important in shielding out solar and cosmic radiation from entering the planet's atmosphere, and is thus crucial for the existence of life on e.g., Earth. Magnetospheres are active and complex systems where the structure and behaviour depends on parameters such as the direction and magnitude of the solar wind, the magnetic moment of the planet's internal magnetic field, sources of magnetospheric plasma, and orientation of the planet's magnetic field (Kivelson and Bagenal, 2007).

Magnetospheric exploration began in the 1950s with rockets launched into the Arctic and Antarctic ionosphere detecting energetic electrons (Kivelson and Russell, 1995). In 1958, Explorer 1 carryied a cosmic ray detector which revealed measurements of the Earth's radiation environment (NASA, a). From these measurements, James Van Allen discovered the radiation belts, consisting of charged particles trapped in space by Earth's magnetic field. Later on, the Explorer 10 and 12 satellites were able to reach further out in space and past the Earth's magnetosphere. These satellites collected measurements essential for understanding the solar wind, and thus the interaction of the solar wind and Earth's magnetic field. In the 1970s, Pioneer 11 and 12 became the first space crafts to reach out to other planets in the solar system; Jupiter and Saturn.

These missions revealed magnetospheres of both planets, later referred to as the Jovian and Kronian magnetosphere (Kivelson and Russell, 1995). While the main structure of Earth's magnetosphere is very similar to the magnetospheres of Jupiter and Saturn, their dynamics differ significantly due to the domination of rotation in the Jovian and Kronian magnetospheres (Kivelson, 2014).

Jupiter and Saturn are not only the largest planets in our Solar System, they are also rapid rotators, that rotates with a period of 9.9 hours, and 10.5 hours, respectively. The moons of Jupiter and Saturn, Io and Enceladus, provides plasma to the Jovian and Kronian magnetospheres. Unlike Earth's magnetosphere, this results in a large amount of internal plasma corotating with the fast rotating magnetopsheres. The combination of fast rotation periods and internal sources of magnetospheric plasma creates a magnetic field structure which looks like a stretched dipole magnetic field. This is referred to as a magnetodisk (Kivelson, 2014), see Fig. 1.1. In 1967, J. A Gledhill was the first one to explain the effects of Jupiter's rapid rotation on the Jovian magnetosphere, and the missions of Pioneer 11 and 12 could reveal the the magnetodisk structure. In 1980, Voyager 1 provided measurements of Saturn's magnetosphere, and Connerney et al. (1981) could therefore reveal an azimuthal current in the Kronian magnetosphere similar to the magnetodisk structure of the Jovian magnetosphere. Throughout the years, the Voyager and Cassini space missions have provided additional in situ measurements of the magnetospheres of the gas giant planets, and several studies of trapped particle dynamics have been carried out.

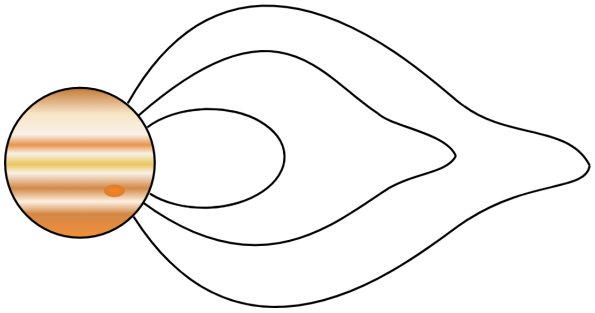

Figure 1.1: Illustration of the magnetodisk magnetic field structure. The dipole magnetic field is radially stretched near the equatorial region at increasing distances from the planet.

While recent observational measurements from rockets and satellites have provided information and further theoretical understanding of planetary magnetospheres, there are still unanswered questions regarding the complex magnetospheric systems. Measurements of space plasma have been important in understanding Earth's magnetosphere, where studies of the dynamics of trapped particles have provided remarkably information about the Van Allen belts. It is known that the Jovian and Kronian magnetospheres share many of the same fundamental structures of Earth's magnetosphere, only that their magnetospheres are extreme in comparison and deviates from a dipole field at distances further out from the planet. How trapped particles behaves along the magnetic fields shaped as a disk in the equatorial region is yet to be investigated and fully understood.

Understanding trapped particle dynamics in a rotating dipole magnetic field is also of interest and particularly timely with the current and future missions to Jupiter; Juno and Juice, as well as the successful missions to Saturn, Cassini. Juno arrived Jupiter in 2016, Juice is planned for launch in 2022, whereas Cassini made its final approach to Saturn in 2017 (NASA, b). The physics of trapped particles in magnetospheres is also a relevant topic to the emerging field of space weather.

In this thesis, a model characterising trapped particle dynamics in a rotating dipole magnetic field is presented. As the magnetodisk structure of the magnetic field of Jupiter and Saturn appears partly as a result of the rotating frame, the thesis will focus on deviations of trapped particle dynamics in a rotating dipole field compared to a non-rotating dipole field. We are therefore to investigate what effect rotation have for trapped particles in the magnetospheres of Jupiter and Saturn.

1.1 Research Question

In 1980, Van Allen and Thomsen (1980) presented a model describing the dynamics of single charged particles in a dipole magnetic field, that is the gyromotion about the magnetic field line, the bounce motion along the field line and the longitudinal drift perpendicular to the field lines. The purpose of this model was to provide parameters that could describe the motion of trapped particles in the magnetosphere of Saturn. In addition to the parameters describing the motion of particles trapped in a dipole magnetic field, additional formulas were provided in order to consider the interaction with Saturn's rings and satellites.

A similar model to Van Allen and Thomsen (1980) which also includes rotation is presented in this thesis. The paper of Van Allen and Thomsen (1980) aimed to provide parameters characterizing the interaction of trapped particles with the rings and satellites of Saturn, but did not include the centrifugal force. In order to account for the rotation, we add the centrifugal force in the guiding centre approximation to the existing model of Van Allen and Thomsen (1980). In this thesis we limit our self to investigate the effect of rotation in a particle's bounce motion only, not the azimuth drift period as well. The following research question will therefore be investigated:

How does the fictitious centrifugal force introduced by a rotating frame of reference influence the bounce motion of a single charged particle trapped in a dipole magnetic field as described by the guiding centre approximation?

1.2 Outline

The thesis is structured in the following way:

Chapter 2 provides the essential theory of trapped particle dynamics in a dipole magnetic field, as well as planetary magnetospheres in more detail and the origin of the magnetodisk.

Chapter 3 presents an analytical derivation of the model characterising bounce period in a rotating dipole magnetic field.

Chapter 4 presents an analysis of the results from chapter 3.

Chapter 5 summarises the work and contains a conclusion.

2

Theoretical Background

The goal of this chapter is to gain overview of the motion of single charged particles trapped in various planetary magnetic fields. To do this, we will review the dynamics of charged particles trapped in a dipolar-like magnetic field. Section 2.1 covers the theory of a dipole magnetic field. In Section 2.2, trapped particle dynamics will be reviewed in light of the guiding centre approximation, and the three adiabatic invariants associated with the periodic motions; magnetic moment, bounce motion, and drift motion. Furthermore in Section 2.3, planetary magnetospheric physics will be surveyed with emphasis on the differences between the magnetosphere at Earth and at the gas giant planets.

2.1 Dipole magnetic field

The magnetic field of the Earth and other magnetised planets are usually approximated to a dipole field configuration when looking at distances that are not too far away from the surface of the planet (Baumjohann and Treumann, 1996). The Earth's magnetic dipole field can be written in terms of latitude λ and radial distance r in a spherical coordinate system, as follows

$$\boldsymbol{B} = \frac{\mu_0}{4\pi}\frac{M_E}{r^3}\left(-2\sin\lambda\hat{\boldsymbol{e}}_r + \cos\lambda\hat{\boldsymbol{e}}_\lambda\right) \tag{2.1}$$

M_E is the dipole moment of the Earth, given as $M_E = 8.05 \cdot 10^{22} Am^2$, $\hat{\boldsymbol{e}}_r$ and $\hat{\boldsymbol{e}}_\lambda$ are unit vectors in radial and latitudinal direction, respectively (Baumjohann and Treumann, 1996). An illustration of the coordinate system can be seen in Fig. 2.1, where the unit vectors in radial and latitudinal direction are indicated as yellow arrows.

From Eq. (2.1) the radial and latitudinal components of the magnetic field can be obtained

$$B_r = -\frac{\mu_0}{4\pi}\frac{M_E}{r^3} 2 \sin\lambda \tag{2.2}$$

$$B_\lambda = \frac{\mu_0}{4\pi}\frac{M_E}{r^3} \cos\lambda \tag{2.3}$$

The strength of a dipole magnetic field at a specific location which is not too far away from the Earth (Baumjohann and Treumann, 1996) is given by

$$B(\lambda) = \frac{\mu_0}{4\pi}\frac{M_E}{r^3}(1 + 3\sin^2\lambda)^{1/2} \tag{2.4}$$

where M_E is the magnetic dipole moment of the Earth, r is the distance from the center of the Earth to the location of interest and λ is the magnetic latitude of the location.

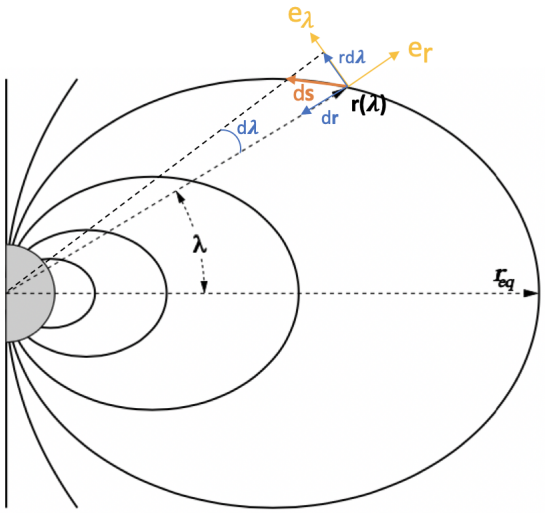

Figure 2.1: Illustration of how the dipole field line equation $r(\lambda)$, in Eq. (2.9), is a function of cosine squared, and how it solely depends on the variables λ – the magnetic latitude, and r_{eq} – the radial distance out to the equatorial plane. Figure adapted from (Baumjohann and Treumann, 1996) and further edited.

2.1.1 Dipole field line equation

The dipole field line equation represents any dipole field line with a radial distance r_{eq} out to the equatorial plane, see Fig. 2.1. If the equatorial distance r_{eq} is known, the distance from the planet out to any point on the field line can be calculated. The following derivation of the dipole field line equation is captured from Baumjohann and Treumann (1996).

The dipole field line equation is obtained from the condition that the magnetic field direction $\boldsymbol{B}$ is parallel to the arc element $d\boldsymbol{s}$ for any given point on the magnetic field line (Prölss, 2004)

$$d\boldsymbol{s} \times \boldsymbol{B} = 0 \tag{2.5}$$

An axisymmetric magnetic dipole field is assumed, as in Fig. 2.1. The condition in Eq. (2.5) can therefore be written in terms of spherical coordinates, with radial and latitudinal direction, $\hat{\boldsymbol{e}}_r$ and $\hat{\boldsymbol{e}}_\lambda$ respectively (Baumjohann and Treumann, 1996)

$$\frac{r d\lambda}{dr} = \frac{B_\lambda}{B_r} \tag{2.6}$$

The radial and latitudinal components of the magnetic field, given in Eq. (2.1), extends Eq. (2.6) into

$$\frac{dr}{r} = -\frac{2\sin\lambda}{\cos\lambda} d\lambda \tag{2.7}$$

Integrating Eq. (2.7) from the radial distance of the equatorial plane r_{eq} where $\lambda = 0$ to an arbitrary radial distance r on the magnetic field line where $\lambda > 0$ we get

$$\int_{r_{eq}}^{r} \frac{1}{r'} dr' = \int_0^\lambda \frac{2d(\cos\lambda')}{\cos\lambda'}, \tag{2.8}$$

Which gives the dipole field line equation

$$r(\lambda) = r_{eq} \cos^2\lambda \tag{2.9}$$

where $r(\lambda)$ is the radial distance from the center of the planet out to the magnetic field line for a given position λ, r_{eq} is the radial distance of the equatorial plane, and λ is the latitude of interest. As the guiding centre moves along a dipole magnetic field line, the dipole field line equation is essential in describing a trapped particle's bounce motion along the field line.

In order to express the ratio of magnetic field strength at equator B_{eq} to magnetic field strength at the mirror point B_m, we can insert the dipole field line equation into Eq. (2.4). That gives

$$B(\lambda) = \frac{\mu_0}{4\pi} \frac{M_E}{r_{eq}^3 \cos^6\lambda} (1 + 3\sin^2\lambda)^{1/2} \tag{2.10}$$

r_{eq} is the radial distance along the equatorial plane measured from the center of the Earth out to the L shell. The L-value for the Earth's magnetic field is given by $L = r_{eq}/R_E$, where R_E is the radius of the Earth. The magnetic field strength is then a function of the magnetic latitude and the L shell

$$B(\lambda, L) = \frac{\mu_0}{4\pi} \frac{M_E}{(LR_E)^3 \cos^6 \lambda} (1 + 3\sin^2 \lambda)^{1/2} \tag{2.11}$$

which can be further simplified as

$$B(\lambda, L) = \frac{B_E}{L^3} \frac{(1 + 3\sin^2 \lambda)^{1/2}}{\cos^6 \lambda} \tag{2.12}$$

where $B_E = \mu_0 M_E / 4\pi R_E^3$ is the equatorial magnetic field on the Earth's surface (Baumjohann and Treumann, 1996). A particular point along a field line is its intersection with the equatorial plane, where the magnetic field strength obtains a minimum $B_{eq} = B_E/L^3$. The ratio of the magnetic field strength at any given point along the field line to the magnetic field strength at the equatorial plane is then

$$\frac{B(\lambda)}{B_{eq}} = \frac{(1 + 3\sin^2 \lambda)^{1/2}}{\cos^6 \lambda} \tag{2.13}$$

From this, we have a relation that describes magnetic field strength on the field line, to magnetic field strength at equator as a function of the magnetic latitude λ.

2.2 Single Particle Motion

To understand the behaviour of trapped particles in planetary magnetic fields, the basics of single particle motion in plasma physics will be covered. Unlike particles in a neutral gas, where it is sufficient to describe the particle motion statistically as a Maxwellian distribution, plasma particles are affected by electromagnetic forces, and thus the detail of the particle's motion becomes important.

2.2.1 Gyration

A charged particle with mass m and charge q in a electromagnetic field will experience the Lorentz force (Öztürk, 2012)

$$\frac{d(\gamma m\boldsymbol{v})}{dt} = q[\boldsymbol{E}(\boldsymbol{r}) + \boldsymbol{v} \times \boldsymbol{B}(\boldsymbol{r})] \tag{2.14}$$

where $\gamma = (1 - v^2/c^2)^{-1/2}$ is the relativistic term, v is the speed of the particle, $\boldsymbol{E}$ is the electric field and $\boldsymbol{B}$ is the magnetic field. Eq. (2.14) describes the particle's motion as a function of position and time.

Assuming no electric field, $\boldsymbol{E} = 0$, and a static and uniform magnetic field $\boldsymbol{B}$, Eq. (2.14) reduces to

$$\frac{d(\gamma m\boldsymbol{v})}{dt} = q[\boldsymbol{v} \times \boldsymbol{B}] \tag{2.15}$$

which shows that the acceleration will stay perpendicular to the velocity at all times, and the speed of the particle is therefore assumed to be constant (Öztürk, 2012). Since the Lorentz force always acts perpendicular to the particle motion, it causes the particle to gyrate.

If the particle's velocity is not perpendicular to the magnetic field, the magnetic force will in stead act perpendicular to the velocity component that is perpendicular to the magnetic field. The parallel velocity component is unaffected by the magnetic force, and will cause the particle to gyrate in a helical motion along the field line. The angle between the particle's velocity and the magnetic field is called the pitch angle, and is defined as

$$\alpha = \arctan\left(\frac{v_\perp}{v_\parallel}\right) \tag{2.16}$$

which is the ratio between the particle's perpendicular velocity component and the parallel velocity component (Baumjohann and Treumann, 1996). The size of the pitch angle is thus affecting the helix path of the particle motion, and is illustrated in Fig. 2.2.

The solution to Eq. (2.15) is the gyro motion of the particle described as a

simple harmonic oscillator, with a cyclotron frequency (Chen, 1974)

$$\omega_c \equiv \frac{|q|B}{\gamma m} \tag{2.17}$$

The particle will gyrate at this frequency with a radius on the size of the Larmor radius r_c, defined as

$$r_c \equiv \frac{\gamma m v_\perp}{|q|B} \tag{2.18}$$

Eq. (2.17) and Eq. (2.18) shows how the gyration of a particle depends on the strength of the magnetic field, and the particle's charge and mass. Particles will gyrate differently depending on its mass and charge, and the magnetic field they are moving in. In example, it will cause heavy ions to gyrate in large circles, and lighter electrons to gyrate in smaller circles. The Larmor radius will additionally depend on the particle's velocity component perpendicular to the magnetic field.

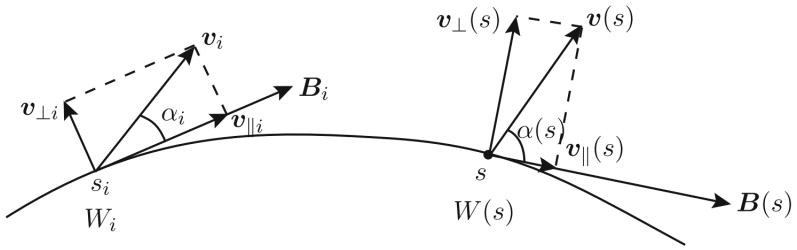

Figure 2.2: Pitch angle α at two points along the magnetic field line, denoted as W_i and $W(s)$, showing the particle's velocity direction and the components parallel and perpendicular to the magnetic field. Figure is adapted from (Roederer and Zhang, 2014).

2.2.2 Guiding centre approximation

Solving the Lorentz force in Eq. (2.14) for a particle's position in a nonuniform magnetic field at every single point of the gyro motion can lead to very complex solutions. The particle's gyro motion is therefore often averaged out so that the particle's overall trajectory is described only as its guiding centre - the centre of its gyration. The particle motion is thus independent of the gyration. Averaging over one gyration period gives the position of the guiding centre $\boldsymbol{X}(t)$. This is

known as the guiding centre approximation.

$$\langle \boldsymbol{x} \rangle = \frac{\omega_c}{2\pi} \int_{t-\frac{\pi}{\omega_c}}^{t+\frac{\pi}{\omega_c}} \boldsymbol{x}(t')dt' = \boldsymbol{X}(t) \tag{2.19}$$

where ω_c is the cyclotron frequency, and $\boldsymbol{x}$ is the position in the gyromotion. This is illustrated in Fig. 2.3. The guiding centre approximation is only valid under the condition that spatial changes in the magnetic field are not significantly large within one gyroradius (Öztürk, 2012). This can be expressed as

$$r_c \ll \frac{B}{|\nabla B|} \tag{2.20}$$

where r_c is the Larmor radius, and ∇B is the spatial change of the magnetic field in three dimensions. In numerical simulations, the guiding centre approximation is highly advantageous as the particle's motion can be resolved for relatively large time steps. However, if the Larmor radius is large enough for the magnetic field to change significantly on that length scale, the guiding centre may not be valid. In that case there will not be a cyclotron motion of the particle. The guiding centre approximation may be violated for highly energetic particles if the gyroradius is too large, and simulating large time steps of the particle's trajectory would fail (Öztürk, 2012).

2.2.3 Magnetic drifts

In the presence of an external force or an inhomogenous magnetic field, the particle will not only move along the field line, but it will also drift relative to the guiding centre. The drift of the guiding center is usually referred to as a magnetic drift, that appears due to the magnetic field the particle is moving in. The following presents the grad-B drift and the curvature drift by the assumption of the guiding centre approximation.

Grad-B drift

The Larmor radius r_c in Eq. (2.18) is inverse proportional to the strength of the magnetic field B, and particles will therefore gyrate in small circles for strong magnetic fields, and in large circles for weak magnetic fields. In the case where the magnetic field strength varies in space, such that there is a magnetic gradient, the particle will have large Larmor radius as it moves into

regions of weaker magnetic field, and small Larmor radius as it moves into regions of stronger magnetic field. This effect causes an overall motion of the particle – a drift, which can be seen in Fig. 2.4. It shows that the particles drift perpendicular to the magnetic gradient as well as they gyrate. This drift is called grad-B drift and is given as

$$v_\nabla = \frac{\gamma m v_\perp^2}{2q} \frac{\boldsymbol{B} \times \nabla B}{B^3} \tag{2.21}$$

The direction of the cross product between the magnetic field direction and the gradient of the field is thus the direction of the particle's drift. Since Eq. (2.21) depends on the charge of the particle, electrons and ions will drift in opposite directions (Baumjohann and Treumann, 1996).

Curvature drift

A particle will drift perpendicular to the magnetic field line also if the magnetic field is curved. When the magnetic field has a curved shape, such as a dipole and the magnetic field of Earth, the drift is caused by a centrifugal force arising from the particle's circular motion in the curved magnetic field. This drift is

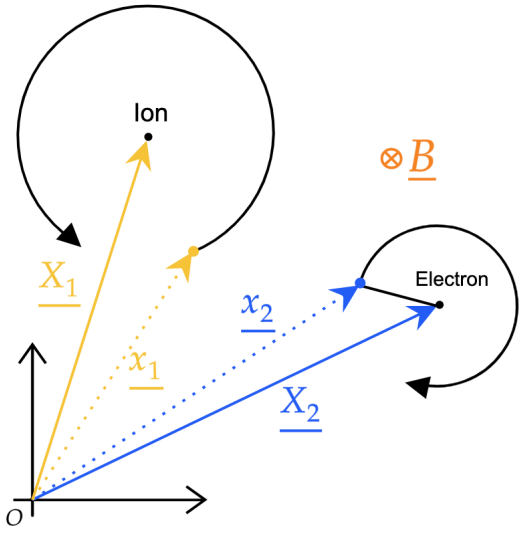

Figure 2.3: Guiding centre for an ion $\underline{X}_1$ and electron $\underline{X}_2$ and its full particle motion $\underline{x}_1$ and $\underline{x}_2$, respectively. The charged particles are present in a static magnetic field pointing in to the page.

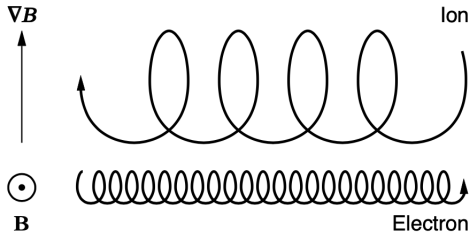

Figure 2.4: Gyro motion for an ion and electron moving in a gradient magnetic field. Figure adapted from (Baumjohann and Treumann, 1996).

given as

$$v_c = \frac{\gamma m v_{\parallel}^2}{q} \frac{\boldsymbol{R}_c \times \boldsymbol{B}}{R_c^2 B^2} \tag{2.22}$$

where $\boldsymbol{R}_c$ is the radius of curvature, and depends on the charge of the particle too, causing electrons and ions to drift in opposite direction.

The combination of a magnetic field that is varying in space, and a magnetic field that is curved, will lead to yet another drift caused by both the gradient magnetic field and the curved magnetic field: a grad-B pluss curvature drift, given as

$$v_c + v_\nabla = \frac{\gamma m}{q} \frac{\boldsymbol{R}_c \times \boldsymbol{B}}{R_c^2 B^2} \left(v_{\parallel}^2 + \frac{1}{2} v_{\perp}^2 \right) \tag{2.23}$$

The Earth's dipole magnetic field is curved and has a gradient since the magnetic field strength decreases with r^3, which causes the trapped particles in Earth's magnetic field to drift azimuthally around the planet. Since the drift is charge dependent, electrons and ions will drift in opposite direction around Earth, thus creating what is known as the ring current (Baumjohann and Treumann, 1996).

2.2.4 Adiabatic invariants

For a trapped particle there are three important periodic motions: the gyromotion around the field line, the bounce motion along the field line, and the drift motion around the planet, see illustration in Fig. 2.5. From adiabatic theory, these periodic motions can be represented in terms of quantities called adiabatic invariants. Adiabatic invariants are quantities that remain approximately constant during small variations of the system within the length scale of the periodicity. If the assumption that the system is varying slowly enough on the length scale of the periodicity is not valid, such as during strong geomagnetically disturbances, the periodic motion of the particle will not hold, and the simplifications cannot be done. The adiabatic invariants are constants of motion, and are derived from the action integral taken over a period (Chen, 1974)

$$J = \oint p \, dq \tag{2.24}$$

where p is the momentum and q is the space coordinate. In space plasma physics there are three adiabatic invariants, each associated to the three periodic motions of a trapped particle; the magnetic moment, the bounce period, and the drift period (Chen, 1974). These invariants will be derived in the following sections. Note that the derivations presented in the following sections of the three adiabatic invariants are similarly discussed as in Öztürk (2012).

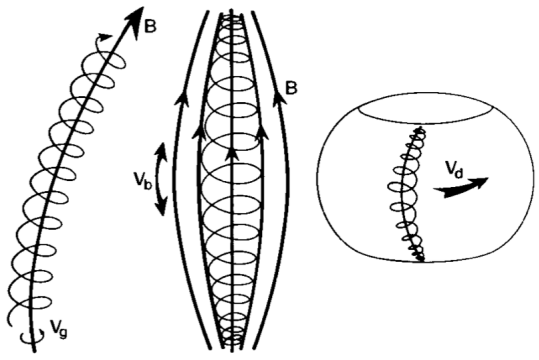

Figure 2.5: Periodic motion of a trapped particle. Figure to the left: Gyro Motion, here denoted as V_g. Figure in the center: Bounce Motion, V_b. Figure to the right: Drift Motion, V_d. The figure adapted from (Kivelson and Russell, 1995).

First adiabatic invariant

The first adiabatic invariant in plasma physics is associated with the magnetic moment. The derivation of the first adiabatic invariant starts with the canonical momentum for a charged particle in a magnetic field, given as

$$J_1 = \oint (\gamma m \boldsymbol{v} + q\boldsymbol{A}) \cdot dl \tag{2.25}$$

where $\boldsymbol{A}$ is the vector potential of the magnetic field and dl is the line element along the particle's gyration path. Here, the magnetic field is assumed to be constant during one integration period of the gyro motion. Eq. (2.25) can further be written as

$$J_1 = \frac{\pi \gamma^2 m^2 v_\perp^2}{qB} \tag{2.26}$$

For a constant mass and charge, we define the magnetic moment,

$$\mu \equiv \frac{1}{2}\frac{\gamma^2 m v_\perp^2}{B} = const. \tag{2.27}$$

which has its name from being equal to the magnetic moment occuring due to the current that is generated from the particle's gyromotion. Eq. (2.27) shows that the magnetic moment stays constant as the particle moves into regions of stronger and weaker magnetic field, because the perpendicular velocity component that changes accordingly. This explains the effect of magnetic mirroring.

Magnetic mirror effect

Magnetic mirroring is the phenomena of particles bouncing back and forth between two mirror points along the magnetic field line. This is due to conservation of energy and magnetic moment, and is caused by a magnetic mirror force acting against the particle's motion. The magnetic mirror force is derived from the Lorentz equation and is defined as the following

$$\boldsymbol{F}_z = -\frac{1}{2}\frac{m v_\perp^2}{B}\frac{\partial \boldsymbol{B}_z}{\partial z} = -\mu \frac{\partial \boldsymbol{B}_z}{\partial z} \tag{2.28}$$

where $\boldsymbol{B}_z$ is the magnetic field in z-direction in cylindrical coordinates, and μ is the magnetic moment. The mirror force will act against the particle's motion

as long as $\frac{\partial B_z}{\partial z} > 0$, hence the negative sign in Eq. (2.28). At the point when the magnetic moment is largest, the force will cause the particle to reflect back towards its direction of motion. The particle is reflected back at the point where its parallel velocity component is zero. Then there is no direction of motion along the field line, only perpendicular to the field line.

For a trapped particle in the dipole magnetic field of Earth, the mirroring effect will occur at the northern and southern hemispheres. The magnetic field strength is strongest at these points due to the converging of the field lines. The magnetic mirroring effect is thus causing a motion of the particle called a bounce motion along the field lines.

Second adiabatic invariant

The second adiabatic invariant is associated with the periodic bounce motion of a trapped particle, which will remain approximately constant as long as the changes in the system is not significantly large within one bounce period. The second adiabatic invariant is derived by integrating the canonical momentum for a charged particle over the path of the guiding field line $\boldsymbol{ds}$.

$$J_2 = \oint (m\boldsymbol{v} + q\boldsymbol{A}) \cdot d\boldsymbol{s} \tag{2.29}$$

where the second term cancels out since it results in the integration of a surface enclosed by a bounce path, which goes back and forth along the same field line. Further on, the second adiabatic invariant is expressed as two times the integration from one mirror point λ_1 to the other λ_2 to complete a full oscillation period of the bounce motion. Eq. (2.29) is then reduced to

$$J_2 = 2 \int_{\lambda_1}^{\lambda_2} m v_{\parallel} ds \tag{2.30}$$

which is an integral of the parallel velocity component along the field line.

Bounce period

A trapped particle's bounce motion is the periodic motion between the two mirror points. The bounce period is determined as the time it takes for the particle to move from the equatorial plane λ_{eq}, to the mirror point at the northern hemisphere λ_m, to the mirror point at the southern hemisphere, and back to the equatorial plane, see illustration in Fig. 2.6. The derivation here is captured from Guio et al. (2020). The bounce period is expressed mathematically as the following (Van Allen and Thomsen, 1980)

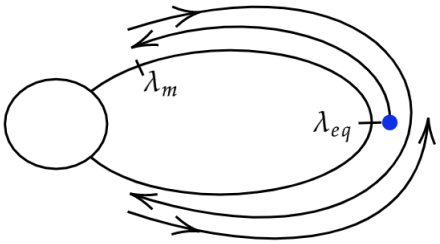

Figure 2.6: Path of a bounce period. To follow the bounce period path, look at the blue starting point at the equatorial plane λ_{eq}, and follow the arrows.

$$\begin{aligned}\tau_b &= 4\int_0^{\lambda_m} \frac{ds}{v_\parallel} \\ &= 4\int_0^{\lambda_m} \frac{ds}{d\lambda}\frac{d\lambda}{v_\parallel}\end{aligned} \tag{2.31}$$

where λ_m is the mirror point magnetic latitude, $v_\parallel$ is the parallel velocity component of the particle, and ds is an arc element along the magnetic field line. The particle's velocity component parallel to the magnetic field is integrated four times from equator, where $\lambda_{eq} = 0$, up to the mirror point magnetic latitude λ_m, in order to complete a full bounce period. The arc element $d\boldsymbol{s}$ along the field line can be expressed in terms of the magnetic latitude of the field line. As explained in Section 2.1 the line element $d\boldsymbol{s}$ along the magnetic field line can be expressed in terms of an infinitesimal radial distance $d\boldsymbol{r}$ and $rd\boldsymbol{\lambda}$ as follows

$$d\boldsymbol{s} = dr\boldsymbol{e}_r + rd\lambda\boldsymbol{e}_\lambda \tag{2.32}$$

The radial and latitudinal components of the magnetic field B_r and B_λ are in the same direction as the unit vectors $\boldsymbol{e}_r$ and $\boldsymbol{e}_\lambda$ and Eq. (2.32) can therefore be expressed as

$$\frac{ds}{d\lambda} = r(\lambda)\left(1 + \frac{B_r^2}{B_\lambda^2}\right)^{1/2} \tag{2.33}$$

The parallel velocity component is derived from conservation of magnetic moment, and is expressed as a function of the total velocity and the magnetic

field at the mirror point B_m and at the position of the particle B

$$v_{\parallel} = v\sqrt{1 - \frac{B}{B_m}} \tag{2.34}$$

By inserting the equation for the arc element in Eq. (2.33) and the parallel velocity in Eq. (2.33) into the bounce period in Eq. (2.31) one gets

$$\begin{aligned}\tau_b &= 4\int_0^{\lambda_m} r(\lambda)\left(1 + \frac{B_r^2}{B_\lambda^2}\right)^{1/2} \frac{1}{v}\left[1 - \frac{B}{B_m}\right]^{-1/2} d\lambda \\ &= 4\frac{\hat{R}_{eq}R_P}{v}\int_0^{\lambda_m} \frac{1}{\hat{R}_{eq}}\left(\frac{1 + B_r^2/B_\lambda^2}{1 - B/B_m}\right)^{1/2} \hat{r}(\lambda)d\lambda\end{aligned}$$

where $\hat{r} = r/R_P$ and $\hat{R}_{eq} = R_{eq}/R_P$, and R_P is the planetary radius. The expression for the bounce period is in Guio et al. (2020) simplified and further expressed as

$$\tau_b = \frac{\hat{R}_{eq}R_P}{v}\Phi(R_{eq}, \alpha_{eq}) \tag{2.35}$$

where Φ is a dimensionless function defined as

$$\Phi(R_{eq}, \alpha_{eq}) = \frac{1}{\hat{R}_{eq}}\int_0^{\lambda_m} r(\lambda)\left(\frac{1 + B_r^2/B_\lambda^2}{1 - B/B_m}\right)^{1/2} \hat{r}(\lambda)d\lambda \tag{2.36}$$

When a dipole magnetic field is assumed, the integral in Eq. (2.36) is usually solved numerically. It is common to approximate the integral as in Baumjohann and Treumann (1996) to $\Gamma = 1.30 - 0.56\sin\alpha_{eq}$. The bounce period can then be expressed in terms of the L shell, $L = r_{eq}/R_P$ as

$$\tau_b \simeq \frac{4LR_P}{v}(1.30 - 0.56\sin\alpha_{eq}) \tag{2.37}$$

which is a function of the equatorial distance r_{eq} and the particle's velocity at equator v_{eq}. This implies that particles further out from the planet are expected

to have a longer bounce period than particles closer to the planet. Particles with low speed at the equatorial plane are expected to have longer bounce periods than particles with high speed.

Electrons will spend seconds to complete a bounce period, while heavier ions will use minutes (Baumjohann and Treumann, 1996). The second adiabatic invariant may therefore be violated for ions with low enough energy under conditions where the magnetic field varies on time scales smaller than the ion bounce period.

Third adiabatic invariant

The third adiabatic invariant is associated with the periodic azimuthal drift motion of trapped particles. As long as any changes to the system are on larger time scales than the period of drift motion, it will be sufficient enough to express the periodicity as an adiabatic invariant. The third adiabatic invariant is derived by integrating the momentum over the path line enclosed by the particle's full orbit around the magnetic dipole, given as

$$J_3 = \oint (m\boldsymbol{v} + q\boldsymbol{A}) \cdot dl \tag{2.38}$$

where dl is a line element along the azimuthal drift path, and $\boldsymbol{A}$ is a vector potential such that $\boldsymbol{B} = \nabla \times \boldsymbol{A}$. Öztürk (2012) shows that the first term is much smaller than the second term, and is therefore cancelled out. The third adiabatic invariant can then be expressed as

$$J_3 = q\Phi \tag{2.39}$$

which describes that the flux the particle encloses as it drifts azimuthally around the dipole is conserved (Baumjohann and Treumann, 1996). The flux Φ is the surface integral of the magnetic field

$$\Phi = \iint \boldsymbol{B} \cdot d\sigma \tag{2.40}$$

where $d\sigma$ is the area enclosed by the orbit of the particle drifting azimuthally around the magnetic field.

Bounce-averaged azimuthal drift period

A trapped particle's drift motion is its azimuthal motion around a dipole magnetic field. The drift motion is an effect of particles which undergo grad-B drift and magnetic curvature drift. The drift is an average of the bounce period,

which is measured as the shift of the angle in azimuth direction during one bounce period, scaled with 2π. The bounce-averaged azimuhtal drift period is given as

$$\tau_d = \frac{2\pi}{\Delta\phi}\tau_b \tag{2.41}$$

where $\Delta\phi$ is a change in longitude direction, and τ_b is the bounce period. Guio et al. (2020) presents the change in longitude during one bounce period, given as

$$\Delta\phi = 4\int_0^{\lambda_m} \frac{v_D}{r\cos\lambda}\frac{ds}{d\lambda}\frac{d\lambda}{v_\parallel} \tag{2.42}$$

where r is the radial distance from the planet to the particle, and v_D is the longitudinal drift velocity of the particle. The longitudinal drift velocity is a combination of magnetic gradient and curvature drift. The derivation of the azimuthal drift period can be found in Guio et al. (2020). The resulting drift period is

$$\tau_d = \frac{2\pi q B_P R_P^2}{3\hat{R}_{eq}\gamma m v^2}\frac{\Phi(R_{eq},\alpha_{eq})}{\Gamma(R_{eq},\alpha_{eq})} \tag{2.43}$$

where $\Phi(R_{eq},\alpha_{eq})$ and $\Gamma(R_{eq},\alpha_{eq})$ are dimensionless functions expressing the bounce period, and the sum of the contributions from the magnetic curvature and gradient drift motions, respectively. For a dipole magnetic field the integral in the dimensionless functions Γ has in Baumjohann and Treumann (1996) been solved numerically. It is approximated to an expression in terms of the L shell, $L = r_{eq}/R_P$, such that the bounce-averaged azimuthal drift period is expressed as

$$\tau_d \simeq \frac{2\pi q B_P R_P^2}{3L\gamma m v^2}\frac{1}{0.35 + 0.15\sin\alpha_{eq}} \tag{2.44}$$

As long as no changes with time scales smaller than the time scale of the drift period τ_b are made to the system, the particle will complete a full drift period around the planet.

2.3 Planetary Magnetospheres

A planet's magnetosphere is the region of plasma that surrounds a planet which is controlled by the planetary magnetic field. The magnetosphere exists due to the interaction between the solar wind and a planet's internal magnetic field.

2.3.1 Formation and structure of a magnetosphere

A combination of the radial flow of the solar wind, and the Sun's rotation results in solar magnetic field lines formed as Archimedean spirals. The opposite polarities of the Sun's magnetic field at the poles results in a current sheet in the equatorial plane, called the heliospheric current sheet, separating the two regions. The sheet has a shape which looks much like the skirt of a ballerina due to the tilt of the Sun's magnetic field (Kivelson and Bagenal, 2007).

Alfvén's theorem states that plasma and magnetic fields are frozen together due to the high conductivity of the plasma. The solar wind will therefore carry the Sun's magnetic field as it escapes the corona. This creates the interplanetary magnetic field (IMF) which reaches out to the planets in our solar system. Another effect of the frozen-in condition is that the Earth's magnetic field remains separated from the IMF. As the solar wind travels at supersonic speeds and interacts with the magnetic field of magnetised planets, a bow shock is created, which slows down the solar wind flow (Kivelson and Bagenal, 2007). This is illustrated in Fig. 2.7. The region just inside the bow shock is called the magnetosheath and consists of shocked solar wind plasma. From the magnetosheath region, particles can further enter a planet's atmosphere through the cusp region. The outer boundary of the magnetosphere is called the magnetopause, and is typically found at distances around $10R_E$ for the Earth on the day side of the planet, where R_E is the radius of Earth. The magnetopause separates shocked solar wind plasma within the magnetosheath from the plasma inside the magnetosphere (Sibeck and Murphy, 2021). When the magnetopause is at balance, the pressure from the solar wind equals the pressure from the planet's magnetic field, and the magnetosphere's size and dynamics is highly influenced by the pressure of the solar wind. Under very intense solar winds, leading to e.g. geomagnetic substorms, the pressure from the solar wind is weaker on the night side of the planet, which results in parts of the magnetosphere to be extended. This is known as the magnetotail, and is illustrated in Fig. 2.7. Alfvén's theorem breaks down during reconnection of the magnetopause in the magnetotail region where the two hemispheres of the magnetosphere meet. This happens only while the direction of the IMF and the planetary magnetic field opposes one another. This process is known as magnetic reconnection. The antiparallel field lines merge, and the plasma mix such that shocked solar wind enters the magnetosphere. While it is yet poorly understood at which location this process happen, magnetic reconnection is the dominant solar wind-magnetosphere interaction (Sibeck and Murphy, 2021). In the inner magnetosphere we find the ring current, the radiation belts and the plasmasphere. Some solar wind particles that entered the magnetopause through the magnetic reconnection process, are further accelerated from the magnetotail to the near-Earth region. In the near-Earth region, at distances from $\sim 1.5 - 9R_E$, ionized particles undergo a curvature-gradient drift, see

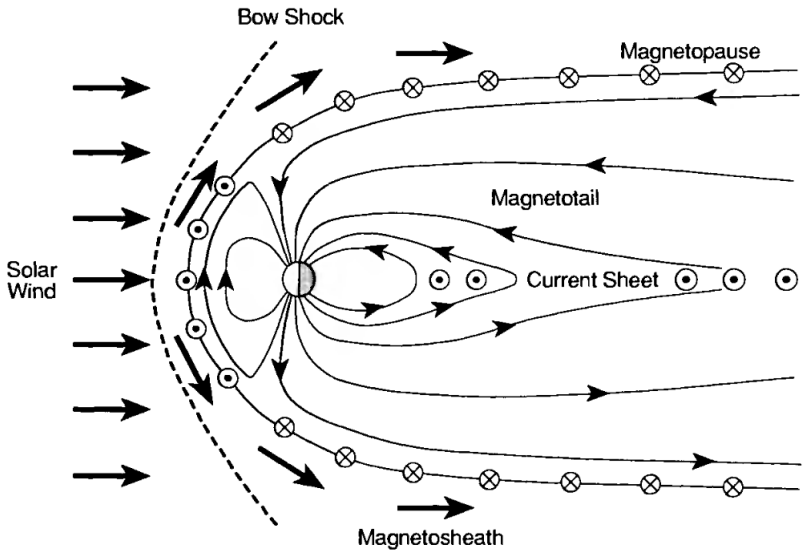

Figure 2.7: Illustration of cross section of Earth's magnetosphere and the interaction with the solar wind. The thin arrowed lines are geomagnetic field lines, and circled dots and cross are curernts. The interaction with the solar wind creates a bow shock. Within this region is the magnetosheath. Further in is the magnetopause which is the boundary of the magnetosphere. The magnetotail and the current sheet are illustrated too. Figure is captured from (Kivelson and Russell, 1995).

Eq. (2.23). As a result, ions with energies of $\sim$ 10 to $\sim$ 200 keV, and electrons with energies of a magnitude lower, will drift in opposite directions around the planet creating the ring current (Sibeck and Murphy (2021), and references therein). Also in the near-Earth region are the two Van Allen radiation belts, more precisely at $1.2 - 2R_E$ for the inner belt and $3 - 7R_E$ for the outer belt. Trapped particles in the magnetospheres constitute the radiation belts, which consists of highly energetic particles of about 1MeV for protons and about 50keV for electrons (Prölss, 2004). Further within this region is the plasmasphere, a cold and dense region where particles mainly originate from the ionosphere with temperatures on the order of $\sim$ 1eV (Kivelson and Bagenal, 2007).

2.3.2 Magnetospheres of the giant planets

The gas giant planets, Jupiter and Saturn, have their names from being the most massive and largest planets in our Solar System, and from being composed of gas rather than solid material. Compared to Earth, Jupiter and Saturn are hundred times as massive and large, with equatorial radii of $R_J \approx 71,500$km and $R_S \approx 60,300$ km, respectively (Achilleos et al., 2021). As Jupiter and

Table 2.1: Planetary magnetic field properties for Earth, Jupiter and Saturn. Magnetic moment at Earth $M_{Earth} = 7.906{\times}10^{25}$ Tesla m^3 [a]. Dipole tilt represents the angle between magnetic and rotation axes[b]. Data is provided in (Kivelson and Bagenal, 2007).

	Earth	**Jupiter**	**Saturn**
r_{eq} (km)	6,378	71,492	60,268
Rot. period (h)	23.934	9.925	10.543
Ions	O^+, H^+	O^+, O^{++}, S^+	O^+, OH^+, $H2O^+$
Mean mass (amu)	1.008	16	17.25
Magnetic moment (M_{Earth})	1[a]	20.000	600
Dipole tilt[b]	+10.8°	−9.6°	−0.0°

Saturn are such massive planets, with $M_J \approx 315 M_{Earth}$ and $M_S \approx 95 M_{Earth}$, respectively, they do not obey the radius-mass relation for solid planets with low mass, given as $R \propto M^{1/3}$. Because of this, they must be gaseous planets, otherwise they would not be as large (D'Angelo and Lissauer, 2018).

Magnetized planets are those planets whose the magnetic field is generated from the electrically conducting fluid in their outer core (Kivelson and Bagenal, 2007). Objects that generate magnetic fields will have a magnetic moment, that describes the strength and orientation of the magnetic field. The magnetic moment of the magnetic field of Jupiter is ∼20,000 times larger than that of Earth's magnetic moment, and for Saturn it is ∼600, indicating enormous internal magnetic fields compared to Earth (Kivelson and Bagenal, 2007). While the Earth's magnetic axis direction of the magnetic north pole is situated close the geographical south pole, with 11° tilt between the magnetic axis and rotation axis. The magnetic axis direction of Jupiter and Saturn is opposite to that of the Earth, such that the magnetic north pole at Jupiter and Saturn is situated close to the geomagnetic north pole, with 9.6° for Jupiter and 0° for Saturn.

While the solar wind is the main source of plasma to Earth's magnetic field, planetary satellites are the main plasma sources in the inner magnetospheres of Jupiter and Saturn. The volcanic moon Io is known for being the primary source of plasma in the Jovian magnetosphere, where erupted lava becomes ionized in the magnetosphere. The mass loading rate of the plasma from Io is $\sim 10^3$ kg s^{-1} (Vasyliunas (2008), and references therein), resulting in mainly sulfur and oxygen ions in the Jovian magnetosphere. In the Kronian magnetosphere, the plumes of the icy moon Enceladus provides plasma to the magnetosphere with a mass loading rate of $\sim 10^2$ kgs^{-1}, which is the reason for water group ions in Saturn's magnetosphere (Achilleos et al., 2021).

The large amount of plasma expelled into the inner magnetospheres of Jupiter and Saturn will corotate with the rotating magnetosphere, and as a result the plasma will shape into a torus around the planet. As Jupiter and Saturn are rapid rotators, where Jupiter rotates with $\sim$ 9.9 hours and Saturn with $\sim$ 10.5 hours, the injected plasma will feel accelerated due to the centrifugal force, originating in the rotating frame, resulting in a strong azimuthal ring current extended radially outwards from the planet. The radially extended ring current will stretch the magnetic field lines in the equatorial plane into a shape referred to as a magnetodisk. A magnetodisk field is a magnetic field that looks like a stretched dipole magnetic field as the field lines are stretched radially in the equatorial plane. The stretching of the field appears at radial distances from the planet where the centrifugal force is largest. At $\sim 6R_J$, where Io is situated, the centrifugal force exceeds the gravitational force by a factor of $\sim$ 20 (Achilleos et al., 2010). From this point, and up to $\sim 20R_J$, the field lines are stretched into a magnetodisk shape. In this region the azimuthal current diffueses into a plasma sheet (Kivelson and Bagenal, 2007). In the Kronian magnetosphere, the centrifugal force exceeds the gravitational force by a factor of $\sim$ 20 at the point of Enceladus, at $4R_S$, resulting in a current that flows azimuthally that stretches the field lines too.

3

Derivation of bounce period in a rotating frame of reference

In order to study how the centrifugal force influences a trapped particle's bounce motion, the effect of rotation must be included in the particle motion along a field line, as described by the guiding centre approximation. How the centrifugal force appears and why it matters for a magnetodisk will be explained in Section 3.1.

The main assumptions in the study of trapped particle dynamics in a rotating frame is conservation of energy and the first adiabatic invariant along the guiding centre path. In a rotating frame it follows that the particle will have a centrifugal potential energy. To account for the centrifugal force in the guiding centre approximation, we must study conservation of kinetic and centrifugal potential energy in a rotating frame. This will be covered in Section 3.2. Conservation of the first adiabatic invariant is essential in the study of a trapped particle's bounce motion as it constrains the particle's perpendicular velocity component along the field line. How conservation of the first adiabatic invariant affects the particle motion in a rotating frame will be discussed in Section 3.2 as well.

In Section 3.3 we will discuss how conservation of energy and the first adiabatic invariant affects the mirror point magnetic latitude in a rotating frame.

Due to the fundamental conservation principles of energy and magnetic moment along the guiding field path, Roederer and Zhang (2014) refer the equatorial plane in the dipole magnetic field as an equilibrium position of the trapped particles. This implies that if one knows the particle's velocity v_{eq}, distance from the planetary axis r_{eq}, and the pitch angle α_{eq}, the particle dynamics along the field line can be calculated analytically thereafter. From this, the particle motion along the field line can be fully understood. The equatorial observations of the particle are thus used as boundary conditions in the model (Roederer and Zhang, 2014). The model presented in this thesis will in addition include one additional boundary condition; the β_{eq} parameter, which will be introduced in Section 3.4.

In Section 3.5, the equation describing the bounce period of a trapped particle in a rotating frame will be presented. The dimensionless function Φ which characterises the bounce period will be the focus in order to answer the research question presented in Section 1.1.

In Section 3.6, we will present what we expect a trapped particle's drift period to be in a rotating frame.

Magnetospheres are complex systems and there are many parameters affecting the dynamics of trapped particles. The following simplifications are done in the derivation of the bounce period in a rotating frame.

- The model in this thesis is an undisturbed dipole magnetic field assumed to be azimuth symmetric about the planet's axis of rotation.

- The trapped particles are assumed to be rigidly corotating with the magnetic field with the angular velocity Ω_p of the planet's rotation (Vogt et al., 2014). The rotation period of the planet is therefore assumed to be constant also at distances further out from the axis of rotation.

- The trapped particles are also assumed to not be drifting azimuthally around the planet. There will only be a bounce motion along the field lines.

3.1 Centrifugal force

A non-inertial frame of reference is a reference system which accelerates relative to an inertial frame. Objects present in such a non-inertial reference frame will therefore be affected by forces due to the acceleration of the frame, called fictitious forces. These forces are fictitious since they have no real physical origin, but only appear since the object is present in the non-inertial frame.

Linear accelerating or rotating frames are examples of non-inertial reference frames, as they move with changing speed or direction relative to the inertial frame. In an accelerating, car a person will feel a force pushing the person back into the seat. If the car is moving in a circular motion with a constant speed, the person will feel a force which pushes the person outwards from the center of the circular motion. To an observer on the outside, there is no origin to each of these forces within the inertial frame. Therefore, the forces experienced by the person in the non-inertial frame are fictitious. There are mainly three fictitious forces in a rotating frame of reference; the Coriolis force, the Centrifugal force and the Euler force, each depending on the angular velocity of the rotating system Ω.

- Coriolis force: $\boldsymbol{F} = -2m\Omega \times \boldsymbol{v}$
- Centrifugal force: $\boldsymbol{F} = -m\Omega \times (\Omega \times \boldsymbol{r})$
- Euler force: $\boldsymbol{F} = -m\frac{d\Omega}{dt} \times \boldsymbol{r}$

In the magnetodisk magnetic field of Jupiter and Saturn, trapped particles will be affected by fictitious forces due to the rotating frame of the rapid rotating planets. The model discussed in this thesis will only include the centrifugal force, we omit the remaining two. The Euler force is ignored since we assume a constant rotation period of the planet, and a stationary orientation of the angular velocity. Because of this, there is no time variation of the angular velocity, and hence $\frac{d\Omega}{dt} = 0$. The Coriolis force is ignored too because it does no work on the particles. It is perpendicular to the particle motion, and will act equally as the magnetic force (Vogt et al., 2014). However, the Coriolis force may have an impact on the drift period, which will be discussed in Section 3.6.

An illustration of the centrifugal force in a system of a rotating dipole magnetic field can be seen in Fig. 3.1, which also illustrates the model derived in this thesis. The resulting centrifugal force F_{CF} is pointing radially outwards from the axis of rotation in a system with angular velocity Ω_p, and a radial distance to the object $\boldsymbol{r} = \boldsymbol{r}_{eq}$. The centrifugal force is proportional to the radial distance of the object, and from the dipole field line equation Eq. (2.9), it follows that the centrifugal force decreases for higher magnetic latitudes. The particles will

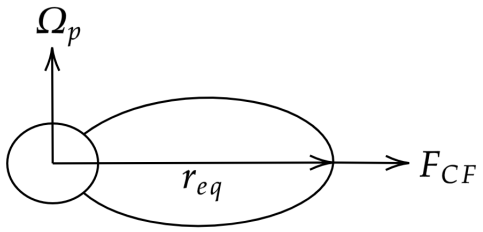

Figure 3.1: Centrifugal force in a system of a rotating dipole magnetic field. Ω_p is the angular velocity of the rotation of the planet, r_{eq} is the radial distance to the magnetic field line at the equatorial plane, and F_{CF} is the resulting centrifugal force.

therefore be subjected to the largest centrifugal force at the equatorial plane.

For trapped particles in a rotating frame, the centrifugal force is defined as

$$\boldsymbol{F}_{CF} = -m\boldsymbol{\Omega}_p \times (\boldsymbol{\Omega}_p \times \boldsymbol{r}), \tag{3.1}$$

where m is the mass of the particle, $\boldsymbol{\Omega}_p$ is the angular velocity of the planet, and $\boldsymbol{r}$ is the radial distance from the axis of rotation out to the point of the particle on the field line.

3.2 Conservation of energy

For a trapped particle bouncing between the mirror points in a rotating dipole magnetic field, energy is conserved along the guiding centre path because the particle is in a conservative vector field. The Lorentz force, originating in the electromagnetic field, is by definition perpendicular to the velocity direction of the particle, and does therefore zero work on the particle. The centrifugal force, originating in the rotating frame, will always act radially outwards from the axis of rotation. That means, along the bounce path, it will therefore be in an angle to the direction of motion, and does zero work on the particle as well.

The trapped particle's total energy along a guiding centre path is the sum of kinetic energy E_K and centrifugal potential energy E_C, and can be thought of as total energy conserved in a spring. Along the guiding centre path, the particle's energy will have the same oscillating behaviour as the spring, where it will have a maximum kinetic energy and a minimum potential energy at equator, whereas a minimum kinetic energy and a maximum potential energy at the mirror point.

Since the centrifugal force in Eq. (3.1) is a conservative force, the centrifugal potential energy E_C can be derived from the condition that a conservative force is the derivative of a potential. From the centrifugal force $\boldsymbol{F}_c$ in Eq. (3.1), we can therefore obtain the centrifugal potential energy E_C from the the following relation

$$\boldsymbol{F}_{CF} = -\nabla E_C \tag{3.2}$$

Solving Eq. (3.2) gives the centrifugal potential energy

$$E_C = -\frac{1}{2}m(\boldsymbol{\Omega}_p \times \boldsymbol{r})^2 + K \tag{3.3}$$

where $\boldsymbol{\Omega}_p$ is the angular velocity of the planet, $\boldsymbol{r}$ is the radial distance from origin to the position of the particle, and K is the integration constant from solving Eq. (3.2). The integration constant K defines the reference point of the centrifugal potential energy and the centrifugal potential energy is negative because it requires work to bring an object towards the axis of rotation (PhysicsLibreTexts).

For the purpose of comparing the particle's kinetic energy to the potential energy, the reference point of the centrifugal potential energy is defined at equator. The constant K is therefore chosen such that the total energy at equator only equals the kinetic energy. The centrifugal potential energy is then expressed as

$$E_C = -\frac{1}{2}m(\boldsymbol{\Omega}_p \times \boldsymbol{r})^2 + \frac{1}{2}m(\boldsymbol{\Omega}_p \times \boldsymbol{r}_{eq})^2 \tag{3.4}$$

A dipole magnetic field is assumed and we insert the dipole field line equation from Eq. (2.9). By solving the cross products in Eq. (3.4), the centrifugal potential energy along the field line can then be expressed as

$$\begin{aligned} E_C(\lambda) &= -\frac{1}{2}m\Omega_p^2 r_{eq}^2 \cos^6\lambda + \frac{1}{2}m\Omega_p^2 r_{eq}^2 \\ &= \frac{1}{2}m\Omega_p^2 r_{eq}^2 (1 - \cos^6\lambda) \end{aligned} \tag{3.5}$$

The resulting expression for the centrifugal potential energy in Eq. (3.5) shows that the centrifugal potential energy is zero at equator where $\lambda = 0$. Furthermore, the centrifugal potential energy increases as $1 - \cos^6\lambda$ towards the mirror point magnetic latitude λ_m.

Recalling the spring analogy, the kinetic energy must decrease as a function of $\cos^6\lambda$ along the guiding path for energy to be conserved. As the particle moves towards higher latitude, the particle's kinetic energy is transformed into potential energy. Hence, the kinetic energy will not be constant along a field line as it is for a non-rotating frame. In order to express the kinetic energy

of the particle along the guiding centre path as a function of the magnetic latitude, we will consider conservation of energy between the equator E_{eq}, and at any arbitrary point along the field line $E(\lambda)$. We know from Eq. (3.5) that the centrifugal potential energy is zero at the equator since this is the reference point of the potential energy. Conservation of energy gives

$$E_{Keq} = E_K(\lambda) + E_C(\lambda) \tag{3.6}$$

where E_{Keq} is kinetic energy at equator, $E_K(\lambda)$ is kinetic energy at a given magnetic latitude λ and $E_C(\lambda)$ is potential energy at a given magnetic latitude λ, see Eq. (3.5). The kinetic energy along the guiding centre path is therefore expressed in terms of kinetic energy at equator and centrifugal potential energy along the guiding centre path

$$E_K(\lambda) = \frac{1}{2}mv_{eq}^2 - \frac{1}{2}m\Omega_p^2 r_{eq}^2(1 - \cos^6\lambda) \tag{3.7}$$

When at equator $\lambda = 0$, the expression in Eq. (3.7) is solely the kinetic energy at the equator, expressed as the equatorial velocity $E_{Keq} = \frac{1}{2}mv_{eq}^2$. As the particle drifts towards higher latitudes, the kinetic energy of the particle will decrease proportional to $\cos^6\lambda$. It is thus clear that rotation will have an effect on the kinetic energy of a trapped particle.

From Eq. (3.5) and Eq. (3.7) it is clear that the particle energy converts between kinetic and potential energy along the guiding centre path depending on the variables v_{eq}, Ω_p and r_{eq}, and behaves as an oscillator along the guiding centre path. From this we observe that kinetic energy obtains a maximum at equator, and a minimum at the mirror point. Furthermore, potential energy obtains a minimum at equator and a maximum at the mirror point.

The particle's total velocity along the field line is given as

$$v_{tot}^2 = v_\perp^2 + v_\parallel^2 \tag{3.8}$$

From conservation of the first adiabatic invariant it follows that the particle's perpendicular kinetic energy is constrained by the magnetic field strength of the field line. When the particle reaches its mirror point at $v_\parallel = 0$, the perpendicular kinetic energy will be at its maximum. From this it follows that perpendicular kinetic energy is maximum where total kinetic energy is minimum. From Eq. (3.8) we can see that the conversion between kinetic and potential energy along the field line will influence the conversion between perpendicular and parallel kinetic energy of the particle. The parallel kinetic energy is thus constrained by both conservation of energy and the first adiabatic invariant. The particle motion along the field line is described by the parallel kinetic energy, and will be shown in Section 3.5.

3.3 Mirror point magnetic latitude

In this section the mirror point magnetic latitude in a rotating frame of reference will be derived by the assumption that energy and the first adiabatic invariant is conserved.

For a particle moving along the magnetic dipole field line as described by the guiding centre approximation, the magnetic mirror point is described in terms of the magnetic field at this point B_m (Guio et al., 2020), see Eq. (2.13). In order to express the mirror point magnetic latitude λ_m in terms of the equatorial pitch angle α_{eq} in a rotating frame, we must first look into conservation of magnetic moment. The following relation is the magnetic moment between the mirror point and the equatorial plane, see Eq. (2.27).

$$\frac{B_{eq}}{B_m} = \frac{v_{\perp eq}^2}{v_{\perp m}^2} = \frac{v_{eq}^2 \sin^2 \alpha_{eq}}{v_m^2} \tag{3.9}$$

Here the pitch angle at the mirror point is 90° thus cancelling out $\sin^2 \alpha_m$. To express the particle's velocity at the mirror point v_m, energy must be conserved between the mirror point E_m and at the equatorial plane E_{eq}, which gives

$$v_m^2 = v_{eq}^2 - \Omega_p^2 r_{eq}^2 (1 - \cos^6 \lambda_m) \tag{3.10}$$

We then get a relation between the magnetic field strength at equator and at the mirror point given as

$$\frac{B_{eq}}{B_m} = \frac{\sin^2 \alpha_{eq}}{1 - \frac{\Omega_p^2 r_{eq}^2}{v_{eq}^2}(1 - \cos^6 \lambda_m)} \tag{3.11}$$

Eq. (3.11) can be simplified by defining a parameter β_{eq}

$$\beta_{eq} \equiv \frac{\Omega_p^2 r_{eq}^2}{v_{eq}^2} \tag{3.12}$$

which also is the ratio of the centrifugal potential energy at the equator to the kinetic energy at the equator. The equatorial pitch angle as a function of the mirror point magnetic latitude is therefore

$$\sin^2 \alpha_{eq} = \frac{B_{eq}}{B_m} \left(1 - \beta_{eq}(1 - \cos^6 \lambda_m)\right) \tag{3.13}$$

Since the particle's centre of gyration is assumed to move along a dipole magnetic field, we can use Eq. (2.13) to express the magnetic field at the equatorial plane B_{eq} to the magnetic field at the mirror point B_m as a function of magnetic latitude λ. We then get

$$\sin^2 \alpha_{eq} = \frac{\cos^6 \lambda_m}{(1 + 3 \sin^2 \lambda_m)^{1/2}} \left[1 - \beta_{eq}(1 - \cos^6 \lambda_m)\right] \tag{3.14}$$

Here we have obtained an expression for the mirror point latitude λ_m for a given equatorial pitch angle α_{eq} in a rotating frame. Eq. (3.14) is a function of the β_{eq} parameter, and it is thus clear that the centrifugal effect will have an impact on the mirror point magnetic latitude of a trapped particle in a rotating frame.

3.4 The β_{eq} parameter

The β_{eq} parameter defined in Eq. (3.12) depends on the angular velocity of the rotating system Ω_p, the equatorial distance r_{eq}, and the velocity of the particle at equator v_{eq}. The three variables in Eq. (3.12) can further be expressed as

$$\Omega_p = \frac{2\pi}{T_p}, \qquad r_{eq} = LR_p, \qquad v_{eq} = \sqrt{\frac{2E_{eq}}{m}} \tag{3.15}$$

where T_p is the rotation period of the planet, L is the L shell value, R_p is the planetary radius of the planet, E_{eq} is the equatorial energy of the particle, and m is the particle's mass. The β_{eq} parameter is thus describing to which degree rotation affects a particle given these conditions.

As the distance from the axis of rotation increases, β_{eq} will increase since it is proportional to r_{eq}^2, see Eq. (3.12). The effect of rotation will therefore have small impact on particles close to the planet. Though as we go further out, rotation will have larger effect on the particles. This would be the case where the equatorial energy and the rotation period is kept fixed as one studies changes in radial direction.

For particles with low equatorial velocity, β_{eq} will be larger compared to particles with high equatorial velocity, since β_{eq} is inverse proportional to v_{eq}^2. The effect of rotation will therefore matter more for a cold plasma population than for a hot plasma population.

For a fast rotating planet, β_{eq} will be larger relative to a planet with a slower rotation, as β_{eq} is proportional to Ω_p^2. Trapped particles in the magnetic field of a fast rotating planet are therefore expected to be more affected by rotation, than trapped particles in a magnetic field of a slow rotating planet.

The centrifugal potential energy will affect the particle dynamics differently depending on how β_{eq} varies. Since β_{eq} is defined as a ratio of the centrifugal potential energy to the kinetic energy at equator, the centrifugal potential energy will have a larger effect for $\beta_{eq} > 1$. When $\beta_{eq} > 1$, the particle will have more potential energy than kinetic energy at equator compared to a

non-rotating frame, and potential energy will dominate the particle dynamics. When $\beta_{eq} < 1$, the particle will have less potential energy than kinetic energy at equator compared to a non-rotating frame, and the centrifugal potential energy will have small effect on the particle dynamics. When $\beta_{eq} = 1$, centrifugal potential energy will have same effect on the particle dynamics as kinetic energy at equator. When $\beta_{eq} = 0$, there will be no rotation as for a non-rotating frame.

3.5 Bounce period

The goal of this section is to derive the final equation describing the bounce period of a trapped particle in a rotating frame of reference. Unlike the derivation of the bounce period in a non-rotating frame in Section 2.2.4, this section will derive a closed form expression of the bounce period by assuming a dipole magnetic field. The dipole field line equation will therefore be used. The bounce period is given by the integral of the inverse parallel velocity, and the next step in the derivation is to express the particle's parallel velocity component.

To obtain the particle's parallel velocity component as a function of the equatorial pitch angle α_{eq}, and the magnetic latitude λ, we must find an expression of the pitch angle α as a function of the equatorial pitch angle α_{eq}. To do so, we assume conservation of magnetic moment between the mirror point and the position of the particle. We also assume conservation of energy between the mirror point E_m and the equatorial region E_{eq}, and we assume conservation of energy between the position of the particle E and the equatorial region E_{eq}. Conservation of magnetic moment gives

$$\frac{B}{B_m} = \frac{v^2 \sin^2 \alpha}{v_m^2} \tag{3.16}$$

By inserting the total velocity v, derived from conservation of energy at equator and at any point along the field line, and the total velocity at the mirror point v_m from Eq. (3.10) we get

$$\sin^2 \alpha = \frac{B}{B_m} \frac{v_{eq}^2 - \Omega_p^2 r_{eq}^2 (1 - \cos^6 \lambda_m)}{v_{eq}^2 - \Omega_p^2 r_{eq}^2 (1 - \cos^6 \lambda)} \tag{3.17}$$

This can be simplified by expressing the pitch angle in terms of β_{eq}.

$$\sin^2 \alpha = \frac{B}{B_m} \frac{1 - \beta_{eq} (1 - \cos^6 \lambda_m)}{1 - \beta_{eq} (1 - \cos^6 \lambda)} \tag{3.18}$$

The numerator in Eq. (3.18) can be replaced by the mirror point magnetic latitude in terms of the equatorial pitch angle in Eq. (3.13), which gives the

pitch angle α as a function of equatorial pitch angle α_{eq}

$$\sin^2\alpha = \frac{B}{B_{eq}}\frac{\sin^2\alpha_{eq}}{1-\beta_{eq}(1-\cos^6\lambda)} \tag{3.19}$$

with this equation, we can obtain an expression for the parallel velocity component.

$$\begin{aligned} v_{\parallel} &= v\sqrt{1-\sin^2\alpha} \\ &= v_{eq}\sqrt{1-\beta_{eq}(1-\cos^6\lambda)}\sqrt{1-\frac{B}{B_{eq}}\frac{\sin^2\alpha_{eq}}{1-\beta_{eq}(1-\cos^6\lambda)}} \end{aligned} \tag{3.20}$$

where the total velocity v, derived from conservation of energy, also is expressed in terms of β_{eq}.

What remains in order to obtain the final equation of the bounce period is to express the arc element ds in the expression of Eq. (2.31). From the expression of the arc element obtained in Eq. (2.33), we insert the radial and latitudinal magnetic field components in terms of a dipole magnetic field as in Eq. (2.2) and Eq. (2.3), as well as the dipole field line equation from Eq. (2.9). This gives the arc element in terms of the equatorial distance r_{eq} and the magnetic latitude

$$\frac{ds}{d\lambda} = r_{eq}\cos\lambda(1+3\sin^2\lambda)^{1/2} \tag{3.21}$$

By inserting the parallel velocity component from Eq. (3.20) and the arc element in Eq. (3.21) we get the final bounce period for a trapped particle in a rotating frame

$$\begin{aligned} \tau_b = 4\frac{r_{eq}}{v_{eq}}\int_0^{\lambda_m} &\frac{\cos\lambda(1+3\sin^2\lambda)^{1/2}}{\sqrt{1-\beta_{eq}(1-\cos^6\lambda)}}\times \\ &\left(1-\frac{(1+3\sin^2\lambda)^{1/2}}{\cos^6\lambda}\frac{\sin^2\alpha_{eq}}{(1-\beta_{eq}(1-\cos^6\lambda))}\right)^{-1/2} d\lambda \end{aligned} \tag{3.22}$$

which is the integral of every magnetic latitude up to the mirror point magnetic latitude λ_m for a given equatorial pitch angle α_{eq}, and now also depending on β_{eq}. The velocity at the equatorial plane, v_{eq}, and the equatorial distance r_{eq} remains constant independently of the mirror point λ, and can therefore be taken out of the integral.

The bounce period in Eq. (3.22) can be simplified to

$$\tau_b = 4\frac{r_{eq}}{v_{eq}}\Phi(\alpha_{eq},\beta_{eq}) \tag{3.23}$$

which resembles the expression for the bounce period in Guio et al. (2020) as defined in Eq. (2.35), but here Φ is a function of β_{eq} as well. The dimensionless function Φ in a rotating frame is then given as

$$\Phi(\alpha_{eq}, \beta_{eq}) = \int_0^{\lambda_m} \frac{\cos\lambda(1+3\sin^2\lambda)^{1/2}}{\sqrt{1-\beta_{eq}(1-\cos^6\lambda)}} \times \left(1 - \frac{(1+3\sin^2\lambda)^{1/2}}{\cos^6\lambda} \frac{\sin^2\alpha_{eq}}{(1-\beta_{eq}(1-\cos^6\lambda))}\right)^{-1/2} d\lambda \tag{3.24}$$

which characterises the bounce period in a rotating frame independently of the equatorial velocity v_{eq} and equatorial radius of the particle r_{eq}.

The dimensionless function Φ expressed in Eq. (3.24) will be the focus in the analysis of this thesis, since it characterises the bounce period, and depends on the β_{eq} parameter. It is therefore of interest to investigate the effect of rotation by considering Φ.

3.6 Drift period

The focus of this thesis is to investigate how the centrifugal force influences the bounce motion of a particle trapped in a rotating frame. However, the drift period in a rotating frame will be presented as it is of interest for future work.

As explained in Eq. (2.41), the particle's drift period is an average of the bounce period scaled with 2π. The change in longitude during one bounce period depends on the particle's magnetic drift around the planet as expressed in Eq. (2.42). In a rotating frame, the particle's drift will additionally be affected by the centrifugal force. This is accounted for when the general force for guiding centre is considered, given as

$$v_F = \frac{1}{q}\frac{\boldsymbol{F}\times\boldsymbol{B}}{B^2} \tag{3.25}$$

which results in the following drift

$$v_{cf} = -\frac{m}{q}\frac{[\Omega\times(\Omega\times\boldsymbol{r})]\times\boldsymbol{B}}{B^2} \tag{3.26}$$

as we see in Eq. (3.26), this drift will be in the same direction as the magnetic drift originating from the grad-B and magnetic curvature drift.

In Section 3.1 it was discussed that the Coriolis force is perpendicular to the particle motion. Since the particle is assumed to move along the field line, the Coriolis force will not do work on the particle. However, as the particle drifts in azimuth direction around the planet, the Coriolis force will act perpendicular to the drift direction, and it may have an impact on the particle's drift. It is mentioned in Vogt et al. (2014) that the Coriolis force will introduce an azimuthal drift averaged over a gyroperiod. If we assume that the Coriolis force will have in impact too, the following drift must be accounted for in a rotating frame of reference

$$v_{cf} = -\frac{2m}{q}\frac{[\Omega \times \boldsymbol{v}] \times \boldsymbol{B}}{B^2} \tag{3.27}$$

which originates from the Coriolis force given as

$$F_c = -2m\Omega \times \boldsymbol{v} \tag{3.28}$$

Given that these assumptions are valid, the resulting azimuth drift for a trapped particle in a rotating frame will be

$$\begin{aligned} v_{rotframe} &= v_{\nabla B} + v_R + v_{cf} \\ &= \frac{m}{q}\left(v_{\parallel}^2 + \frac{1}{2}v_{\perp}^2\right)\frac{\boldsymbol{R_c} \times \boldsymbol{B}}{R_c^2 B^2} + \frac{m}{q}\frac{[\Omega \times (\Omega \times \boldsymbol{r})] \times \boldsymbol{B}}{B^2} \end{aligned} \tag{3.29}$$

where $v_{\nabla B}$ is the grad-B drift, v_R is the curvature drift, and v_{cf} is the drift due to the centrifugal force.

In order to derive a closed form expression of the drift period in a rotating frame as for the bounce period in Section 3.5, we would in this case include the total guiding centre drift in a rotating frame from Eq. (3.29) to the equation for the drift period in Eq. (2.41).

4

Analysis

The bounce period in a rotating frame derived in Eq. (3.22) aims to answer the research question in this thesis. In order to investigate how the centrifugal force influences the bounce motion of a trapped particle in a dipole magnetic field, the focus will be to analyse how the dimensionless function Φ varies with the β_{eq} parameter.

Firstly, the function Φ will be investigated when $\beta_{eq} = 0$. This is done to check the validity of the bounce period expression derived in Eq. (3.22), as if there was no rotation. This will be discussed in Section 4.1.

Further on, in order to analyse how Φ varies with increasing value of β_{eq}, we must first understand how the parallel velocity and the mirror point varies with β_{eq}, since Φ is defined as the integral over the inverse parallel velocity integrated up to λ_m as seen in Eq. (3.24). How the particle energy affects the motion along the field line and the mirror point is presented in Section 4.2.

As discussed in Section 4.2, the parallel velocity and the mirror point magnetic latitude varies depending on the equatorial parameters; E_{eq}, L and Ω_p, which describes the β_{eq} parameter. How β_{eq} varies for hot and cold plasma populations, radial distance from the planetary axis, and different planetary rotation periods is presented in Section 4.3.

How the mirror point magnetic latitude varies with β_{eq} will be discussed in Section 4.4. The inverse parallel velocity will also vary with β_{eq}, and this will

be discussed in Section 4.5.

The main goal of this chapter is to analyse how the dimensionless function Φ varies with β_{eq}. This will be done by comparing the mirror point latitude from Section 4.4 with the inverse parallel velocity in Section 4.5. This is discussed in Section 4.6.

Some particles may not remain trapped along the field line, but will be lost in the atmosphere. This is known as the loss cone. How the effect of rotation influences the loss cone will be covered in Section 4.7.

4.1 Validation of expression

If $\beta_{eq} = 0$ in Φ for a rotating frame derived in Eq. (3.24), we would expect Φ to behave equally as if there was no rotation. In order to validate the model, Φ is plotted for $\beta_{eq} = 0$ in Fig. 4.1 together with the approximated function $\Gamma = 1.30 - 0.5\sin(\alpha_{eq})$ as stated in Baumjohann and Treumann (1996). From Fig. 4.1 we can see that the expression of the dimensionless function in Eq. (3.24) is a good approximation to the numerical expression from Baumjohann and Treumann (1996). It is therefore reasonable to say that the expression for Φ is valid in expressing a particle's bounce period in a non-rotating frame for $\beta_{eq} = 0$.

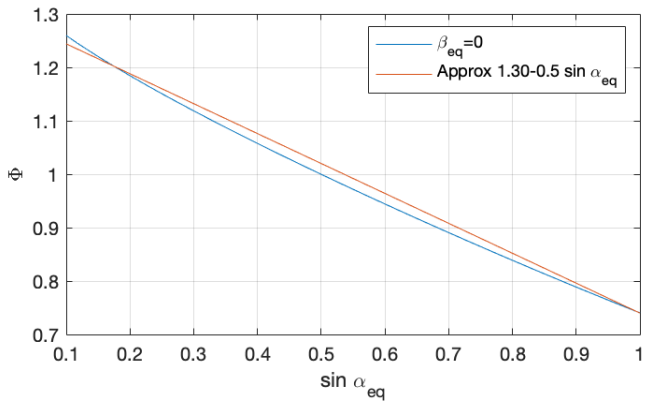

Figure 4.1: Comparison between dimensionless function Φ when $\beta_{eq} = 0$, and numerical approximation of integral $1.30 - 0.5\sin(\alpha_{eq})$ as stated in Baumjohann and Treumann (1996).

4.2 Particle Energy

The kinetic energy of a particle in a rotating reference frame is not constant along the field line. As discussed in Section 3.2, the kinetic energy converts into potential energy along the guiding centre path. The kinetic energy along a field line will decrease as a function of $\cos^6 \lambda$, see Eq. (3.7). How much the kinetic energy decreases depends on the scaling of the equatorial parameters: the equatorial energy E_{eq}, the planetary angular velocity Ω_p, and the L shell value L. Fig. 4.2 illustrates how the kinetic energy, normalised to the equatorial kinetic energy, decreases along the guiding centre path for three different equatorial energies. Fig. 4.2a shows E_{eq} = 500eV, Fig. 4.2b shows E_{eq} = 5keV, and Fig. 4.2c shows E_{eq} = 50keV. The normalised kinetic energy is shown from equator where $\lambda = 0°$ to $\lambda = 14°$ in Fig. 4.2a, and from $\lambda = 0°$ to $\lambda = 70°$ in Fig. 4.2b and Fig. 4.2c. The kinetic energy is also shown for no rotation, see blue line in Fig. 4.2, which agrees with a constant kinetic energy along the field line in a non-rotating frame. From these figures, it is clear that the effect of rotation influences the particle's energy.

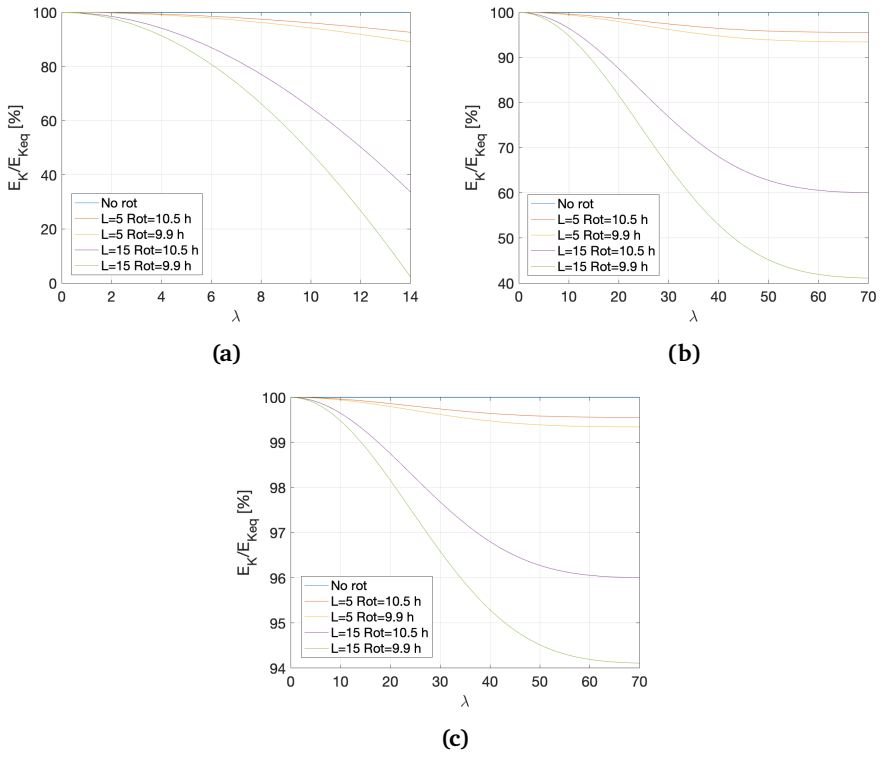

Figure 4.2: Kinetic energy normalised to kinetic energy at equator decreasing with increasing values of the magnetic latitude. The range of magnetic latitude varies with the equatorial kinetic energy (a) E_{eq} = 500eV (b) E_{eq} = 5keV (c) E_{eq} = 50keV.

Low energy particles will loose more of its kinetic energy and gain more potential energy than high energy particles as they drift towards higher latitudes. A particle rotating around Jupiter with a rotation period of 9.9 hours, an equatorial energy of $E_{eq} = 500$eV, at $L = 15$, will have lost 50% of its equatorial kinetic energy at a magnetic latitude of $\lambda = 10°$, see Fig. 4.2a. An equivalent particle with higher energy $E_{eq} = 5$keV, will have lost 50% of its equatorial kinetic energy at $\lambda = 50°$, see Fig. 4.2b. A particle with a higher energy, $E_{eq} = 50$keV, will have lost only 6% of its equatorial kinetic energy at around $\lambda = 70°$, see Fig. 4.2c. From this we can conclude that the centrifugal effect has a lesser impact on particles with high equatorial energy. The kinetic energy is transformed into centrifugal potential energy at a faster rate along the guiding centre path for low energy particles than high energy particles.

The further out from the planet a particle is, the more does the kinetic energy decrease as the particle drifts towards higher latitudes. This is seen when we compare $L = 5$ and $L = 15$ in the plots of Fig. 4.2. A particle with $E_{eq} = 5$keV will have lost much more of its kinetic energy at a distance $L = 15$, then at a distance $L = 5$. This is independent of the equatorial kinetic energy, and can be seen in all of the subplots of Fig. 4.2. Additionally, the kinetic energy decreases faster for a faster rotating planet. For each of the given L shells, the kinetic energy reduces more rapidly when the rotation period is 9.9h compared to 10.5h. Another remark from Fig. 4.2 is how the combination of the distance from the planet, and the rotation period of the planet, affects the kinetic energy. A faster planetary rotation period will cause more kinetic energy to be converted into potential energy at distances further away from the planet, compared to distances close to the planet. In Fig. 4.2b, at $L = 5$, the difference between the kinetic energy for Saturn and Jupiter is very small around 3%, while at $L = 15$, the difference is about 20%. The interpretation of this is that the centrifugal effect has a larger impact on the conversion between potential energy and kinetic energy when the particle is further out from the planet and/or corotates around faster rotating planets.

In this section it has been illustrated that kinetic energy decreases along the field line as an effect of rotation. How much and how fast the kinetic energy converts into potential energy varies with the equatorial parameters L, Ω_p and E_{eq}. The particle's kinetic energy indicates the trapped particle dynamics along the guiding centre path as it describes the particle energy parallel and perpendicular to the magnetic field. The particle motion of a trapped particle bouncing between the mirror points is always on the field line, and it is therefore of interest to study the parallel kinetic energy.

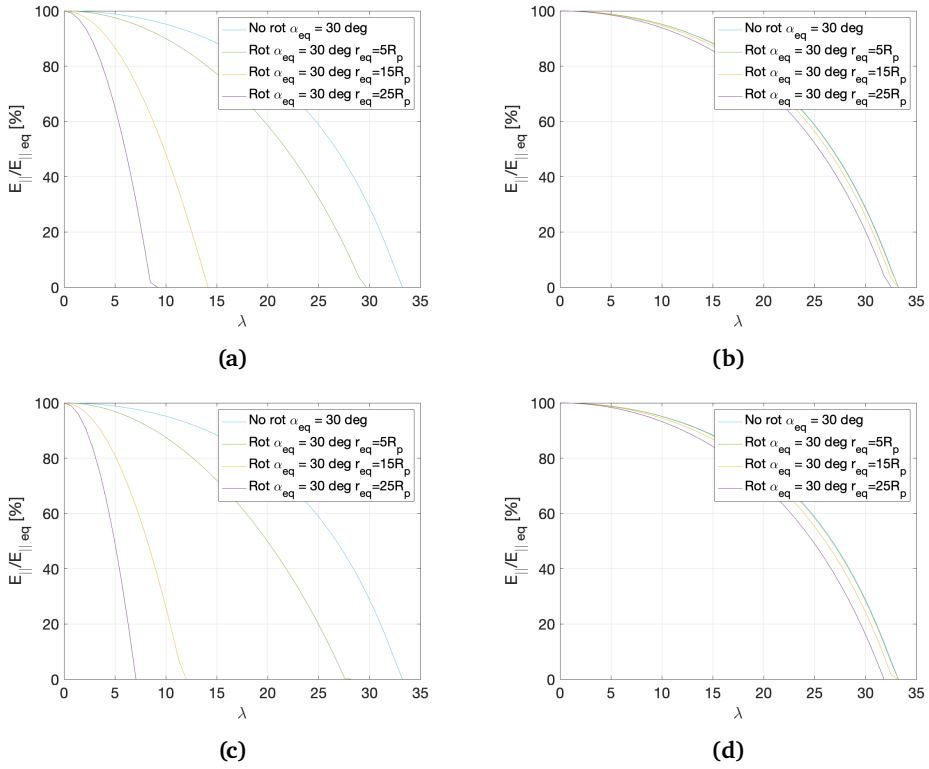

Figure 4.3: Parallel kinetic energy normalised to its value at equator decreasing towards zero for increasing value of magnetic latitude. The equatorial pitch angle is $\alpha_{eq} = 30°$ which explains why the range of magnetic latitude is from $\lambda = 0° - 35°$. (a) Saturn $E_{eq} = 500$eV (b) Saturn $E_{eq} = 50$keV (c) Jupiter $E_{eq} = 500$eV (d) Jupiter $E_{eq} = 50$keV

4.2.1 Parallel kinetic energy

In a rotating frame of reference, Eq. (3.20) states that the parallel kinetic energy along the field line is in addition to the pitch angle, also a function of the L shell, E_{eq} and the angular velocity of the planet Ω_p. Fig. 4.3 shows how the parallel kinetic energy in a rotating frame decreases to zero at different rates depending on these variables. The two plots at the top of the figure shows the parallel kinetic energy for Saturn, while the two plots at the bottom shows for Jupiter. The parallel kinetic energy in a non-rotating frame is also shown in Fig. 4.3, only as a function of α_{eq} and E_{eq} as it is independent of the radial distance from the planet in the non-rotating frame.

The parallel kinetic energy decreases to zero faster at distances further out from the planet. This clearly in seen in Fig. 4.3a and Fig. 4.3c which shows Saturn and Jupiter for $E_{eq} = 500$eV, respectively. At $L = 5$ in Fig. 4.3a, the

parallel kinetic energy has reduced to half of its initial speed around $\lambda = 23°$, whereas at $L = 15$ the parallel kinetic energy has reduced to half of its initial speed around $\lambda = 10°$. For $L = 25$ this happens at about $\lambda = 7°$. The same behaviour is seen for Jupiter in Fig. 4.3c. From Fig. 4.3a and Fig. 4.3c it can also be seen that there is a gap between the curves representing $L = 5$ and $L = 15$. From this it can be understood that the kinetic energy will decrease at a even faster rate at very large distances from the surface of the planet.

The parallel kinetic energy will also decrease to zero faster for cold plasma particles than for hot plasma particles. This is seen when we compare the two plots on the left to the plots on the right in Fig. 4.3. The plots on the left side shows Saturn and Jupiter when $E_{eq} = 500$eV, while the ones on the right illustrates the same for $E_{eq} = 50$keV. At $L = 25$, the kinetic energy has reduced to half of its initial speed at about $\lambda = 7°$ for a cold plasma particle, while this occurs at $\lambda = 26°$ for a hot plasma particle. Compared to a non-rotating frame, the particle at $L = 25$ will have half of its initial speed at 20° lower for a cold plasma particle, but about 3° lower for a hot plasma particle. From this it is clear that the centrifugal effect has larger influence for a cold plasma population than a hot plasma population.

The parallel kinetic energy is also decreasing at a faster rate depending on the planet's rotation period. This can be seen by comparing the plots at the top to the plots at the bottom in Fig. 4.3 which illustrates the parallel kinetic energy of Saturn and Jupiter, respectively. While a cold plasma particle at a distance $L = 25$ reduces to half its energy at around $\lambda = 7°$ for Saturn, this happens at around $\lambda = 5°$ for Jupiter. For a hot plasma particle this is around $\lambda = 26°$ for Saturn compared to around $\lambda = 25°$ for Jupiter. The difference is very small since Jupiter and Saturn rotates with relatively equal rotation periods. However, we can conclude that the centrifugal effect will be larger for rapid rotating planets.

From studying the plots in Fig. 4.3 it is evident that parallel kinetic energy converts into perpendicular kinetic energy at different rates depending on the parameters L, E_{eq} and Ω_p. This results in different points of reflection of the trapped particle, and the mirror point depends on these variables too. This has been shown in the expression for the equatorial pitch angle in a rotating frame, derived in Eq. (3.14), and will be discussed in the following subsection.

4.2.2 Mirror point

The mirror point magnetic latitude is the point where the particle's parallel velocity component has reached zero. How fast the parallel kinetic energy decreases to zero is therefore affecting the particle's mirror point. Fig. 4.4

shows how the mirror point varies for both Saturn and Jupiter as a function of equatorial energy E_{eq}, the equatorial pitch angle α_{eq}, the distance from the planet r_{eq}, and the planet's rotation period. The energies are ranging from cold to hot plasma, from 10 keV to 1 MeV at fixed equatorial pitch angle of $\alpha_{eq} = 30°$, and with three equatorial distances $r_{eq} = 5R_p$, $10R_p$, $20R_p$, in the case of no rotation. The yellow line in Fig. 4.4 shows the mirror point magnetic latitude λ_m when there is no rotation and is constant for any value of r_{eq} and E_{eq}. Note that the yellow line covers the blue and the red line, each representing different equatorial distances for the non-rotating frame. This shows that the mirror point magnetic latitude in a non-rotating frame is independent of the equatorial parameters L, E_{eq} and Ω_p.

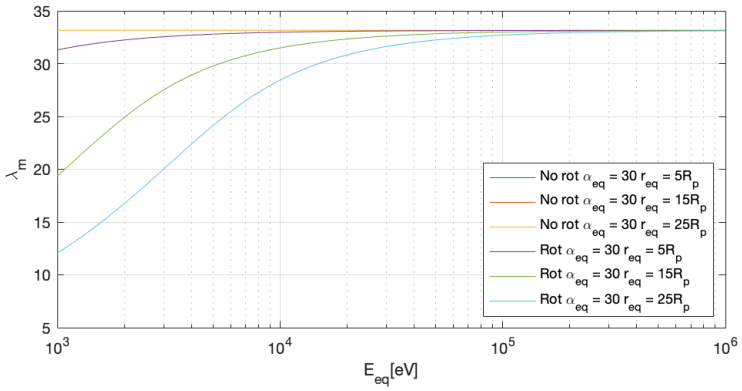

(a) Saturn

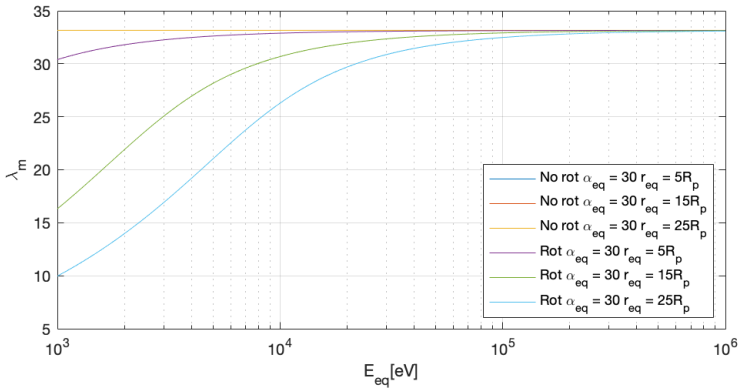

(b) Jupiter

Figure 4.4: Comparison of mirror point magnetic latitude λ_m between Saturn and Jupiter, and how it varies for changing equatorial energy E_{eq}. The equatorial energy E_{eq} is ranging from 10 keV to 1 MeV, where the equatorial pitch angle is set to $\alpha_{eq} = 30°$. Three equatorial distances are chosen $r_{eq} = 5R_p$, $15R_p$, $25R_p$ in the case of rotation and no rotation.

The mirror point depends on the particle's equatorial energy E_{eq}, resulting in a broader range of mirror points for a cold plasma population, than for a hot plasma population. The range of mirror points for cold plasma extends from $\lambda_m = 31°$ for $L = 5$ to $\lambda_m = 13°$ for $L = 25$. The range narrows as the equatorial energy increases up to around 10^5eV, where the mirror point becomes independent of the distance from the planet, and is $\lambda_m = 35°$ like the non-rotating frame of reference. The hot plasma particles will bounce at the nearly the same magnetic latitude, independently of the distance from the planet, while the cold plasma particles will bounce at mirror points that are strongly affected by the distance from the planet. Cold plasma particles are therefore more affected by the centrifugal force than hot plasma particles.

We can see how the mirror point magnetic latitude also depends on the planet's rotation period by comparing Fig. 4.4a and Fig. 4.4b which shows Saturn and Jupiter respectively. Trapped particles corotating around Jupiter will bounce at lower magnetic latitudes than trapped particles corotating around Saturn. This effect is most clear in the range of cold plasma population where the mirror point is $\lambda_m = 13°$ for Saturn but $\lambda_m = 10°$ for Jupiter, at $L = 25$. The differences between the mirror points of Jupiter and Saturn is seen for every equatorial energy in Fig. 4.4. However, in the range of hot plasma population from 10^5eV to 10^6eV, it is clear that these plasma particles are not affected by the planet's rotation period either.

From the investigations in these plots it has been shown how the conversion between kinetic energy and potential energy will affect the parallel kinetic energy and thus the magnetic mirror point. It has been shown that the centrifugal effect will impact the parallel kinetic energy and the mirror point at different rates depending on the variables E_{eq}, the L shell and the rotation period of the planet. Another important remark from these results is how the centrifugal effect does not only influence each variable individually, but also that the combination of the variables emphasizes the impact of the centrifugal effect. The combination of these variables represents β_{eq}, as defined in Eq. (3.12). In the next section, the β_{eq} parameter will be presented. It will be shown how β_{eq} depends on the variables E_{eq}, the L shell and the rotation period of the planet. Understanding how β_{eq} behaves is essential for the study of a trapped particle's bounce motion in a rotating frame of reference.

4.3 The β_{eq} parameter

The β_{eq} parameter is a measure of how much a particle with the given equatorial conditions; Ω_p, L and E_{eq}, is affected by the centrifugal force. In this section, the β_{eq} parameter will be studied in terms of how it varies for hot and cold

plasma populations, as a function of radial distance from the planetary axis, and for different planetary rotation periods. Fig. 4.5 shows how β_{eq} varies for Jupiter and Saturn from cold plasma $E_{eq} \sim 10^2$eV to hot plasma $E_{eq} \sim 10^6$eV, and for L shell values from $L = 5$ to $L = 20$. The β_{eq} parameter expands from $\beta_{eq} = 0$ to $\beta_{eq} = 35$, whereas the surface plot is shown in logarithmic scale.

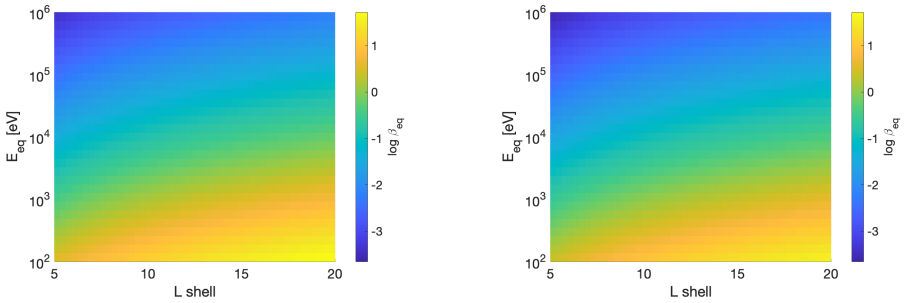

(a) Jupiter **(b)** Saturn

Figure 4.5: Logarithmic plot of the β_{eq} parameter as a function of L shell value and equatorial energy E_{eq}.

It is clear from Eq. (3.12) that β_{eq} is proportional to r_{eq}^2, and β_{eq} is therefore expected to increase further out from the planetary axis. By considering β_{eq} solely as a function of the L shell, Fig. 4.5 shows that for every given value of the equatorial energy E_{eq}, β_{eq} increases for increasing value of L. This is as expected, which also agrees with the fact that centrifugal potential energy increases with distance from the planetary axis. This is because it requires more work to bring the particle back to the planet at far distances. From this, we can see that the centrifugal effect is larger for particles further out from the planet.

The β_{eq} parameter is by definition inverse proportional to v_{eq}, and β_{eq} is therefore expected to be large for a cold plasma population, and smaller for a hot plasma population. If we also consider β_{eq} solely as a function of the equatorial energy E_{eq}, we can from Fig. 4.5 observe that for each L shell, β_{eq} decreases as the energy increases. From this, we can understand that the centrifugal effect is larger for particles with low equatorial energy than particles with high equatorial energy.

The β_{eq} parameter is also proportional to the planet's angular velocity Ω_p^2, and is expected to increase for faster rotating planets. When comparing the surface plots of β_{eq} for Jupiter and Saturn in Fig. 4.5a and Fig. 4.5b, β_{eq} is larger for both E_{eq} and L for Jupiter than for Saturn. The difference of β_{eq} in the two plots is not large, but is a result of their relatively equal rotation periods ~ 9.9

hours and $\sim$ 10.5 hours. The centrifugal effect will be larger for faster rotating planets.

In the region where particles will have more potential energy than kinetic energy, and the centrifugal potential energy will dominate the particle dynamics is in Fig. 4.5 referred to as the region where green turns over to yellow. The green region is where $\beta_{eq} \approx 1$ and the yellow region is where $\beta_{eq} \gg 1$. This is in the region mainly of the cold plasma population, but also for hotter plasma at further distances around $L = 15$ and $L = 20$. For the green and yellow region, β_{eq} ranges from 1 to 35 at its maximum at $L = 20$. The centrifugal potential energy will therefore dominate the kinetic energy for cold plasma particles, and even more for those particles further out from the planet. This indicates that the dynamics of cold plasma particles is dominated by the centrifugal force, and results in cold plasma particles being pulled out in radial direction at a larger rate than they will be able to bounce along the field line.

In the region where particles will have more kinetic energy than potential energy, which is not enough for the centrifugal potential energy to dominate the particle dynamics is in the region where green turns over to blue. This is in the region of hot plasma population. The hot plasma population is more spread than the cold plasma population, ranging from about 10^3eV to 10^6eV, whereas the cold plasma population is only on the order of $\sim 10^2$eV. The blue region in Fig. 4.5 shows β_{eq} values in the range of $3.4 \cdot 10^{-3}$ to 0.02, which is approximately zero, where the smallest value is at $L = 5$. From this it can be understood that the hot plasma population is almost not affected by the centrifugal force, independently of the distance from the planetary rotation axis.

In reality, it is shown that the corotation of the magnetospheric plasma in the rotating system is varying as a function of the radial distance in the magnetosphere (Hill, 1979). The rotation frequency is possibly decreasing by an order of 2 from the surface of the planet to the magnetopause. We would therefore not expect β_{eq} to necessarily increase proportional to r_{eq}^2 in a real life scenario. To take this into account in the β_{eq} parameter, we would in that case expect the effect of rotation to have a smaller effect for particles further out from the planet. That is at distances where the corotation of the magnetospheric plasma is significantly lower than the angular frequency of the planet.

In this section it has been shown that β_{eq} varies as a function of the equatorial parameters of a trapped particle, that is L, E_{eq} and Ω_p. β_{eq} describes to which degree the centrifugal potential energy dominates the dynamics of the particle, and the dynamics of the particle in a rotating frame will therefore depend on the particle's equatorial parameters. The particle dynamics will be more

affected by rotation if the particle has a low equatorial velocity, is further out from the surface of the planet, or corotates with the angular frequency of a rapid rotating planet.

4.4 Mirror point and the β_{eq} parameter

In a rotating frame, the mirror point magnetic latitude λ_m is not only a function of the equatorial pitch angle as in a non-rotating frame, but also a function of β_{eq}. This was shown in Eq. (3.14). The point where the particle bounces back depends on how much kinetic energy is converted into potential energy along the guiding centre path. Fig. 4.6 shows a surface plot of how the mirror point varies as a function of the equatorial pitch angle and β_{eq}. For $\beta_{eq} = 0$ the mirror point behaves as studied for a non-rotating frame where small equatorial pitch angles results in high mirror points, while large equatorial pitch angles results in low mirror points. As β_{eq} increases towards 1, we can observe the same behaviour, only that the mirror point becomes lower at even smaller values of the equatorial pitch angle. In the range where $\beta_{eq} > 1$, and towards $\beta_{eq} \approx 5$, the mirror point decreases significantly for low pitch angle values. For values of $\beta_{eq} = [15, 35]$ the mirror point is low, about $\lambda_m = 10°$ for all pitch angles. The interpretation of this is that the effect of rotation results in low mirror points also for small pitch angles. The mirror points becomes lower for smaller and smaller pitch angles as β_{eq} increases. This effect becomes significant in the region where $\beta_{eq} > 1$, which is the point where the centrifugal potential energy dominates the kinetic energy. The kinetic energy converts to potential energy at a faster rate when $\beta_{eq} > 1$ than for $\beta_{eq} = 0$. Particles will therefore not drift to high latitudes even with small pitch angles as they are strongly affected by the radial pull of the centrifugal force.

In this section it has been shown that the mirror point magnetic latitude is reduced as an effect of rotation. We showed that the mirror point magnetic latitude varies as a function of β_{eq} as well as the equatorial pitch angle α_{eq}. As β_{eq} increases, the mirror point magnetic latitude will be lower for small equatorial pitch angles. It was shown that the mirror point latitude reduces faster for small equatorial pitch angles in the region around $\alpha_{eq} < 30°$, compared to $\alpha_{eq} > 30°$.

4.5 Parallel velocity component $v_{\parallel}$

In this section we want to study how the particle's inverse parallel velocity component increases towards infinity along the guiding centre path as β_{eq}

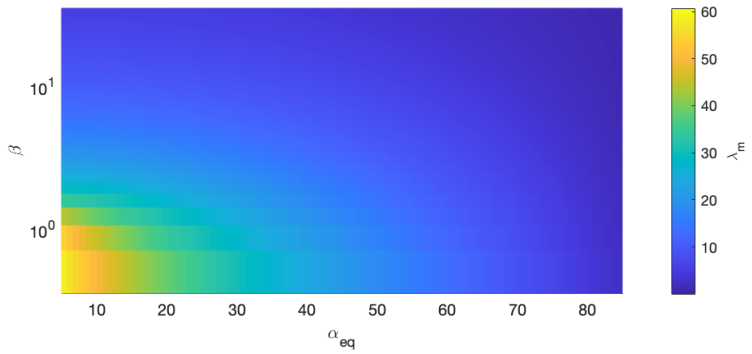

Figure 4.6: Mirror point latitude λ_m as a function of equatorial pitch angle α_{eq} and the β_{eq} parameter.

increases. The mirror point latitude is the point where the parallel velocity component is zero. The point where the particle is reflected back is therefore at the asymptote of the inverse parallel velocity component. How the inverse parallel velocity increases as a function of magnetic latitude is shown in Fig. 4.7a1 – Fig. 4.7a4. The four plots illustrate the inverse parallel velocity with and without rotation, and for $\beta_{eq} = \{0.4, 1, 2.5, 3.7\}$. The plots show two equatorial pitch angles $\alpha_{eq} = 10°$ and $\alpha_{eq} = 60°$, in order to study how the inverse parallel velocity increases differently for small and large equatorial pitch angles.

Fig. 4.7a1 – Fig. 4.7a4 illustrate that the inverse parallel velocity component increases towards its asymptote at a faster rate as β_{eq} increases. The inverse parallel velocity will increase faster as β_{eq} increases, for both values of α_{eq}. However, the inverse parallel velocity increases faster when $\alpha_{eq} = 10°$ than for $\alpha_{eq} = 60°$. When we compare $\beta_{eq} = 0.4$ to $\beta_{eq} = 2.5$ in Fig. 4.7, we can see that the inverse parallel velocity has increased significantly more when $\alpha_{eq} = 10°$ than for $\alpha_{eq} = 60°$. When $\alpha_{eq} = 10°$ and $\beta_{eq} = 0.4$, the asymptote is at around $\lambda = 49°$ compared to $\lambda = 52°$ in a non-rotating frame. While when $\beta_{eq} = 2.5$, the asymptote is at around $\lambda = 22°$ compared to $\lambda = 52°$ in the non-rotating frame. When $\alpha_{eq} = 60°$ and $\beta_{eq} = 0.4$, the asymptote is at around $\lambda = 12°$ compared to $\lambda = 14°$ in a non-rotating frame. While when $\beta_{eq} = 2.5$, the asymptote is at around $\lambda = 8°$ compared to $\lambda = 14°$ in the non-rotating frame. This shows that the inverse parallel velocity increases towards its asymptote faster for small pitch angles than large pitch angles when β_{eq} increases. The mirror point is thus reducing faster for small pitch angles than large pitch angles, which is in agreement to what we could see in Fig. 4.6.

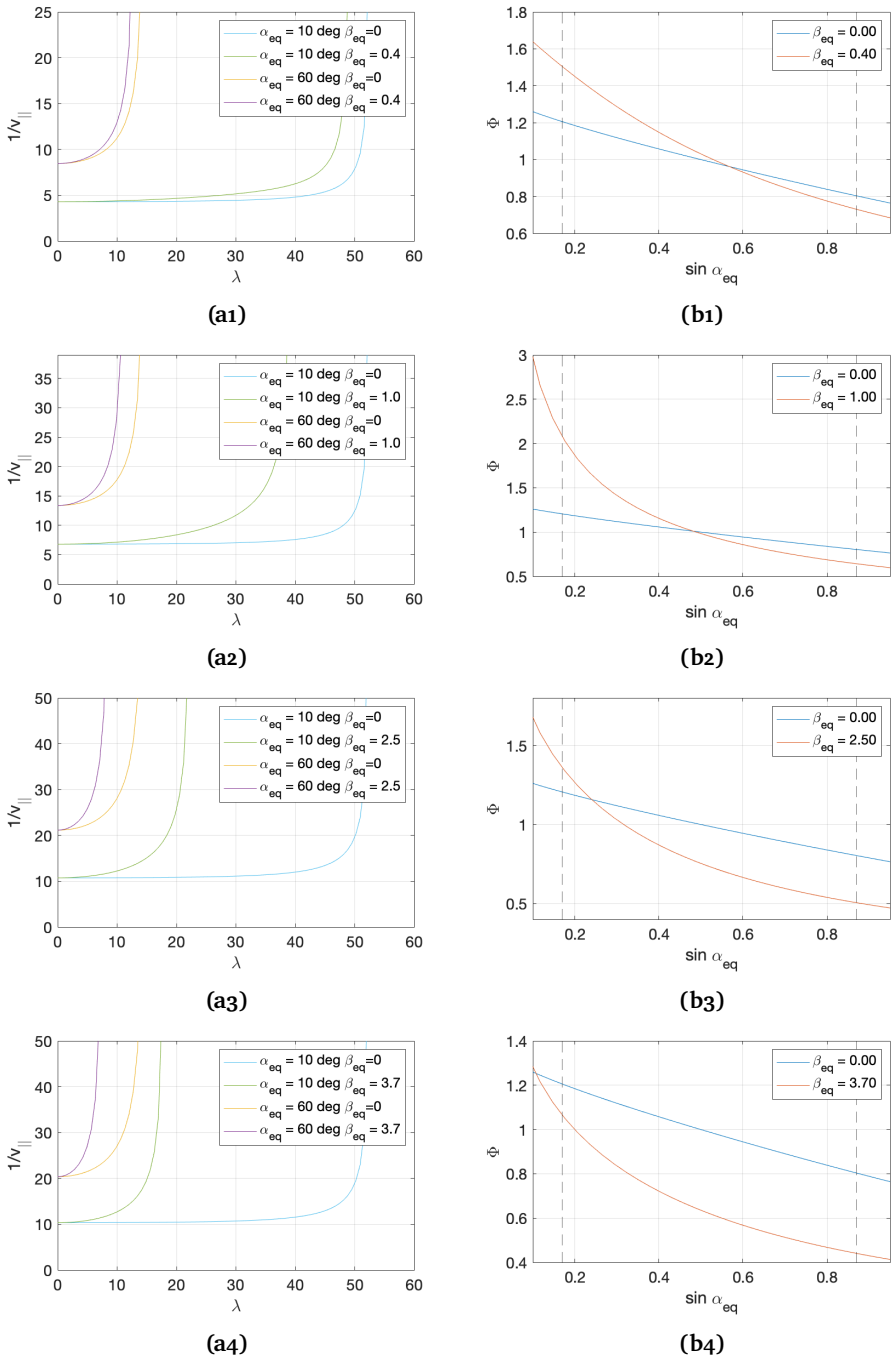

Figure 4.7: (a1) - (a4) shows how the inverse parallel velocity component increases as a function of magnetic latitude for four values of the β_{eq} parameter. That is $\beta eq = 0.4, 1, 2.5$ and 3.7. The inverse parallel velocity is shown for $\alpha_{eq} = 10°$ and $\alpha_{eq} = 60°$, for rotation and no rotation. The values of the inverse parallel velocity are normalized by 10^5m/s. The initial value of the parallel velocity at equator affects the β_{eq} parameter, and is the reason for the different scaling on the y axes. (b1)-(b4) shows the resulting dimensionless function Φ integrated over equatorial pitch angles ranging from $\sin \alpha_{eq} = 0.1-1$ for the same four β_{eq} values. The vertical dotted lines are at the two points of $\alpha_{eq} = 10°$ and $\alpha_{eq} = 60°$, that is $\sin \alpha_{eq} = 0.17$ and $\sin \alpha_{eq} = 0.87$ resp. The dimensionless function Φ is also shown for when there is no rotation that is $\beta_{eq} = 0$.

4.6 Dimensionless function Φ

The goal of this section is to analyse how the parallel velocity component in combination with the mirror point latitude influences the dimensionless function Φ as the β_{eq} parameter increases. As seen in Section 4.4 and Section 4.5, the parallel velocity component and the mirror point depend on β_{eq}. How the parallel velocity and the mirror point varies with β_{eq} is thus essential in the analysis of Φ. We now limit the investigation to distinct β_{eq} values, while we in the previous sections referred to how it varies with the planet's rotation, the L shell value, and the equatorial energy of the particle.

Fig. 4.7b1 – Fig. 4.7b4 show how Φ varies in range of $\sin(\alpha_{eq}) = 0.1 - 1$ as the β_{eq} parameter increases. The four plots show $\beta_{eq} = \{0.4, 1, 2.5, 3.7\}$. The function Φ is shown for rotation and no rotation for the purpose to study the effect of rotation. The two functions Φ for rotation and no rotation intersect at different pitch angles as β_{eq} increases. When $\beta_{eq} = 0.4$, they intersect at $\sin(\alpha_{eq}) = 0.55$, which corresponds to $\alpha_{eq} \approx 33°$. For larger values of β_{eq}, they intersect at $\alpha_{eq} \approx 26°$, $\alpha_{eq} \approx 14°$ and $\alpha_{eq} \approx 6°$ for $\beta_{eq} = 1, 2.5$ and 3.7, respectively. On the left side of the crossing we observe that Φ is larger in a rotating frame, than in a non-rotating frame. On the right side of the cross we observe that Φ is smaller than in a non-rotating frame. How much larger and how much smaller Φ is compared to the non-rotating frame, does also vary with β_{eq}.

At which rates the inverse parallel velocity increases and the mirror point latitude decreases is determined by β_{eq}, as discussed in Section 4.4 and Section 4.5. If the inverse parallel velocity increases faster than the mirror point reduces, the resulting function Φ will be larger compared to a non-rotating frame. If the inverse parallel velocity does not increase faster than the mirror point is reducing, the resulting function Φ will be less compared to a non-rotating frame. By knowing this, we can relate the plots which show the inverse parallel velocity in Fig. 4.7a1 – Fig. 4.7a4 to the plots showing the dimensionless function in Fig. 4.7b1 – Fig. 4.7b4. In order to compare how the inverse parallel velocity in combination with the mirror point influences the dimensionless function Φ, we will focus on two pitch angle values, $\alpha_{eq} = 10°$ and $\alpha_{eq} = 60°$. The points of these pitch angles are drawn as vertical dotted lines in Fig. 4.7b1 – Fig. 4.7b4, at $\sin(\alpha_{eq}) = 0.17$ and $\sin(\alpha_{eq}) = 0.87$.

First we study $\alpha_{eq} = 10°$ which is the dotted line on the left side. When $\beta_{eq} = 0.4$ the asymptote of the inverse parallel velocity only has reduced from around $\lambda = 52°$ to $\lambda = 49°$, which is not significantly low, see Fig. 4.7a1. The inverse parallel velocity will increase at a faster rate which results in a larger function Φ compared to a non-rotating frame, see the dotted line to the left in Fig. 4.7b1. The function is $\Phi = 1.45$ for $\beta_{eq} = 0.4$ while it is $\Phi = 1.2$ for

$\beta_{eq} = 0$. As expected, Φ is therefore larger in a rotating frame. When $\beta_{eq} = 2.5$ we observe the same behaviour for $\alpha_{eq} = 10°$. Even though we observe the asymptote of the inverse parallel velocity to be much smaller when $\beta_{eq} = 2.5$, the inverse parallel velocity has increased at a sufficient rate for the function Φ to be larger compared to a non-rotating frame. On the other hand when $\beta_{eq} = 3.7$, the asymptote has reduced significantly from the non-rotating frame. The inverse parallel velocity is not increasing fast enough, and the resulting Φ is lower than in a rotating frame. From this it is clear that particles with small pitch angles will bounce at high latitudes additionally as their speed will decrease faster than in a non-rotating frame. Particles with small pitch angles will therefore spend longer time completing a bounce period compared to a non-rotating frame as long as β_{eq} is not too large.

We will now study $\alpha_{eq} = 60°$ which is the dotted line on the right side. When $\beta_{eq} = 0.4$, the asymptote has decreased only about 2° in latitude compared to the non-rotating frame. However, we observe the resulting function Φ to be lower than in a non-rotating frame, which is because inverse parallel velocity has not increased significantly within the time the mirror point has reduced. For $\beta_{eq} = 1$ and $\beta_{eq} = 2.5$ we observe the same behaviour, and the resulting Φ is lower than in a non-rotating frame. When $\beta_{eq} = 3.7$, we observe the same behaviour too, only here the resulting Φ is much lower than the non-rotating frame. The mirror point has reduced remarkably, and the inverse parallel velocity has not increased at a fast rate compared to the non-rotating frame. From this is clear that particles with large equatorial pitch angles are trapped closer to the equatorial region as an effect of rotation. Compared to a non-rotating frame, the time it takes to complete a bounce period is therefore shorter as β_{eq} increases.

An important remark from the analysis of the plots in Fig. 4.7 is how the combination of increasing inverse parallel velocity and decreasing mirror point also depend on the equatorial pitch angle α_{eq} as β_{eq} increases. As we have studied, the mirror point latitude will decrease more rapidly than the inverse parallel velocity will increase when β_{eq} increases, which will also concern smaller α_{eq} as β_{eq} gets larger. This effect is seen as the intersection between Φ for rotation and no rotation appears at lower equatorial pitch angles as β_{eq} increases. To further study and understand how Φ also varies with the equatorial pitch angle, the next step is to investigate Φ in terms of both β_{eq} and α_{eq}.

Fig. 4.8 shows how the dimensionless function Φ evolves for different pitch angles as β_{eq} increases. The values of the equatorial pitch angles in Fig. 4.8 are $\alpha_{eq} = \{10°, 20°, 30°, 40°, 70°\}$. The function Φ is normalised to its value when there is no rotation $\Phi/\Phi_{\beta_{eq}=0}$. As β_{eq} increases, the normalised function Φ peaks for equatorial pitch angles up to around $\alpha_{eq} = 30°$. The peak of $\alpha_{eq} = 10°$

appears at $\beta_{eq} = 1$, while for larger equatorial pitch angles, the peaks appear at lower values of β_{eq}. For equatorial pitch angles larger than about 30°, there is no peak and Φ only decreases as β_{eq} increases. The horisontal dotted line indicates where Φ equals its value in the non-rotating frame, $\Phi_{\beta_{eq}=0}$.

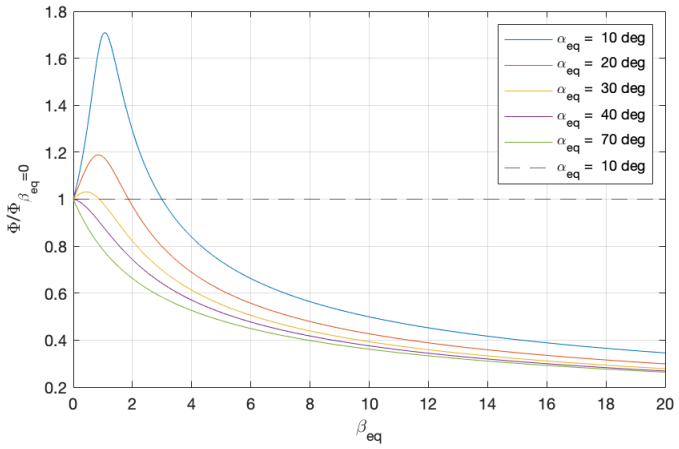

Figure 4.8: Dimensionless function Φ, normalised to its value when $\beta_{eq} = 0$, as a function of $\beta_{eq} = 0-20$ and equatorial pitch angles $\alpha_{eq} = 10°, 20°, 30°, 40°$ and 70°. The horisontal dotted line indicates where Φ and $\Phi_{\beta_{eq}=0}$ are equal.

Above and below the dotted line in Fig. 4.8 describes when the resulting function Φ is larger and smaller than what it would be in non-rotating frame, given the equatorial pitch angle α_{eq} and β_{eq}. The interesting part in Fig. 4.8 is the shape of Φ above the dotted line, where we observe peaks of Φ for different pitch angles. In the following, we will therefore focus on how Φ behaves as a function of β_{eq} in the region above the dotted line which concerns particles with equatorial pitch angles with $\alpha_{eq} < 30°$. We know that β_{eq} is a rate that describes to which degree the system is affected by rotation. Furthermore, β_{eq} describes the relation between centrifugal potential energy at equator to kinetic energy at equator, and we will now study how Φ varies in relation to this.

When $\beta_{eq} < 1$, a trapped particle will have more centrifugal potential energy and less kinetic energy at equator compared to a non-rotating frame. Since the energy of the particle converts between kinetic energy and potential energy along the guiding centre path, the particle will have more centrifugal potential energy as it moves to higher latitudes, than at equator. As an effect of rotation, the parallel velocity will therefore reduce faster compared to a non-rotating frame. However, as we discussed in Section 4.4, these pitch angles are small enough for the mirror point to not reduce significantly since $\beta_{eq} < 1$. From this it is clear that Φ increases in the region of $\beta_{eq} = (0, 1)$, and peaks at $\beta_{eq} = 1$ for the lowest α_{eq}.

When $\beta_{eq} = 1$, the centrifugal potential energy equals the kinetic energy at equator. Kinetic energy will therefore convert into potential energy along the field line faster than when $\beta_{eq} < 1$. $\beta_{eq} = 1$ is the point where the normalised function Φ peaks, that is for the smallest equatorial pitch angle $\alpha_{eq} = 10°$ in Fig. 4.8. The peak of the normalized function Φ is the maximum time a particle will spend on a bounce period given the equatorial pitch angle. Note that maximum time means maximum time normalised to the non-rotating frame. When $\beta_{eq} = 1$ we observe the largest distribution of Φ values across the equatorial pitch angles which range from $\Phi = (0.7, 1.7)$. What this means is that the outcome of the bounce period will vary significantly depending on the particle's equatorial pitch angle when $\beta_{eq} = 1$.

When $\beta_{eq} > 1$, centrifugal potential energy will be larger than kinetic energy at equator. Along the guiding centre path, this means that kinetic energy will convert into potential energy much faster than when $\beta_{eq} = 1$. Since the total velocity is given by $v_{tot}^2 = v_\perp^2 + v_\parallel^2$, it follows that the parallel velocity will decrease more rapid and the mirror point as well. As discussed in Section 4.4 the mirror points will be lower also for small pitch angles when $\beta_{eq} > 1$, which will impact the resulting bounce period. This is why we observe Φ to decrease past $\beta_{eq} = 1$ for the lowest α_{eq}.

For large enough values of β_{eq}, which is below the dotted line, centrifugal potential energy is a lot larger than kinetic energy at equator. Kinetic energy will therefore convert into potential energy at an even faster rate than discussed above. The effect of rotation causes the mirror point to reduce significantly, and the inverse parallel velocity is not increasing fast enough. The function Φ is thus smaller than in a rotating frame, and is the reason why we observe Φ to only decrease below this point. Note that the horisontal dotted line in Fig. 4.8 indicates where the function Φ for $\beta_{eq} = 0$ intersects the function Φ when $\beta_{eq} > 0$ in Fig. 4.7. From this, one can interpret when Φ and $\Phi_{\beta_{eq}=0}$ are equal, as the limit where centrifugal potential energy will dominate the particle dynamics such that the particle is trapped closer to equator than in a non-rotating frame.

At which β_{eq} the function Φ equals its initial value when $\beta_{eq} = 0$, and intersects the dotted line, is plotted in Fig. 4.9 as a function of equatorial pitch angles. Fig. 4.9 shows that equatorial pitch angles smaller than $\alpha_{eq} = 40°$ will intersect the dotted line for different values of β_{eq}. This implies that for smaller equatorial pitch angles it requires a larger β_{eq} for the centrifugal effect to dominate the particle dynamics. When $\alpha_{eq} = 10°$, β_{eq} must be larger than 3 for the centrifugal effect to dominate the dynamics of particles with $\alpha_{eq} = 10°$ and larger. For equatorial pitch angles larger than $\alpha_{eq} = 40°$, the function Φ does not cross the dotted line which is seen as $\beta_{eq} = 0$ in Fig. 4.9 for these pitch angles.

The function Φ does therefore not peak for $\alpha_{eq} > 40°$. These pitch angles are large enough to remain trapped in the region close to equator independently of β_{eq}.

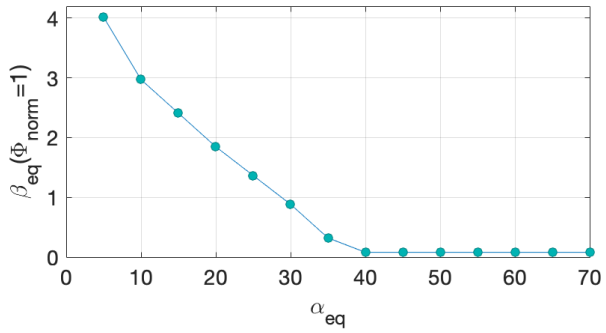

Figure 4.9: β_{eq} values required for centrifugal effect to dominate the particle dynamics for a given α_{eq}. This is when Φ, normalised to its value when there is no rotation $\beta_{eq} = 0$, equals 1, seen as the dotted line in Fig. 4.8. The β_{eq} values are shown as a function of equatorial pitch angles ranging from $\alpha_{eq} = 5° - 70°$.

A more complete view of how Φ varies as a function of both β_{eq}, and the equatorial pitch angle α_{eq}, is shown in Fig. 4.10. The plot is shown in logarithmic scale to emphasize variations in Φ. There is a clear difference above and below $\beta_{eq} = 1$. For values of $\beta_{eq} < 1$, we observe a similar behaviour as in a non-rotating frame where the bounce period is longer for small pitch angles and shorter for large pitch angles. However, as β_{eq} increases towards $\beta_{eq} = 1$, we observe a larger variation of Φ for the pitch angles as discussed in Fig. 4.8. At $\beta_{eq} = 1$ we observe a peak region of small pitch angles too. For values of $\beta_{eq} > 1$, we observe Φ to be lower also for small α_{eq} as discussed previously. For very large values of β_{eq}, closer to $\beta_{eq} = 10$, the bounce period is shorter almost independently of the equatorial pitch angle.

From the investigations in this section it is clear that as β_{eq} increases, the mirror point latitude decreases, and the inverse parallel velocity increases. How these two variables change in relation to each other as β_{eq} increases determines the bounce period of a trapped particle. The effect of rotation results in longer bounce periods for particles with small α_{eq} and shorter bounce periods for particles with large α_{eq}, compared to a non-rotating frame. It has also been shown that the effect of rotation will result in shorter bounce periods for particles with smaller α_{eq} when β_{eq} increases. As we could see in Fig. 4.9, the value of β_{eq} needed for centrifugal force to dominate the particle dynamics increases for smaller α_{eq}. Values of β_{eq} larger than the limit as shown in Fig. 4.9 will result in shorter bounce periods compared to a non-rotating frame.

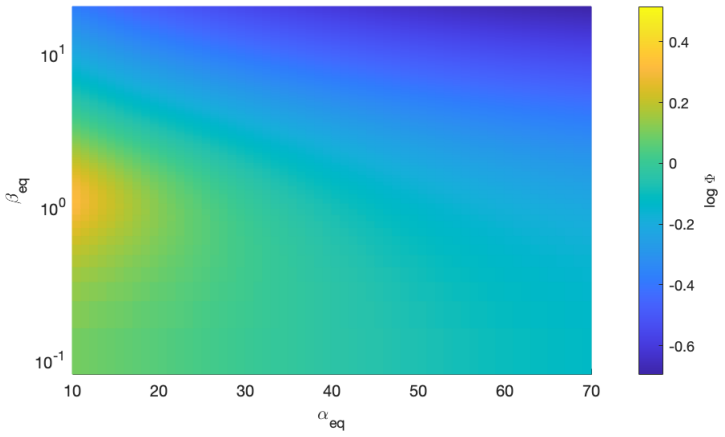

Figure 4.10: Dimensionless function Φ as a function of the equatorial pitch angle α_{eq} and the β_{eq} parameter. The surface plot is shown in logarithmic scale to emphasize variations in Φ.

4.7 Loss cone

For small enough equatorial pitch angles some trapped particles may be lost to the atmosphere. These particles have mirror points which are too far down in the atmosphere for them to collide with the neutral particles (Baumjohann and Treumann, 1996). In a rotating frame, the range of particles lost to the atmosphere will change. The following equation shows how the equatorial loss cone α_l is also a function of β_{eq} in a rotating frame.

$$\sin^2 \alpha_l = \frac{\cos^6 \lambda_E}{(1 + 3\sin^2 \lambda_E)^{1/2}}(1 - \beta_{eq}(1 - \cos^6 \lambda_E)) \tag{4.1}$$

Following the derivation in Baumjohann and Treumann (1996), it can be simplified to

$$\sin^2 \alpha_l = (4L^6 - 3L^5)^{-1/2}(1 - \beta_{eq}(1 - L^{-3})) \tag{4.2}$$

which shows that the equatorial loss cone is a function determined by the L shell and the β_{eq} parameter. Since Eq. (4.2) depends on β_{eq}, the particles lost to the atmosphere will be valid only for given energy values, L shell values and rotation periods. How the equatorial loss cone varies with E_{eq}, L and Ω_p is not straightforward. However, the solution to Eq. (4.2) is plotted in Fig. 4.11 as a function of β_{eq} when there is no rotation, and when $\beta_{eq} = \{0.2, 0.4, 0.6, 0.8\}$.

Fig. 4.11 shows how the range of equatorial loss cone values reduces as β_{eq} increases. From Section 4.6 we know that the effect of rotation confines particles towards equator. What we have seen is that also particles with small equatorial pitch angles will be trapped closer to equator as β_{eq} increases. Since particles bounce to lower latitudes in a rotating frame, we expect less particles to be lost to the atmosphere. From this, it is clear why we observe the range of equatorial loss cone values to reduce as β_{eq} increases.

The range of loss cone values in Fig. 4.11 is not shown for β_{eq} values larger than $\beta_{eq} = 0.8$. For $\beta_{eq} > 0.9$, the solution to Eq. (4.2) is not valid. Since centrifugal potential energy dominates kinetic energy at equator when $\beta_{eq} > 1$, the effect of rotation may be sufficiently large at this point for particles with small α_{eq} to be trapped closer to equator. If this results in that no particles are lost to the atmosphere, it is likely the reason we get no solution for $\beta_{eq} > 0.9$.

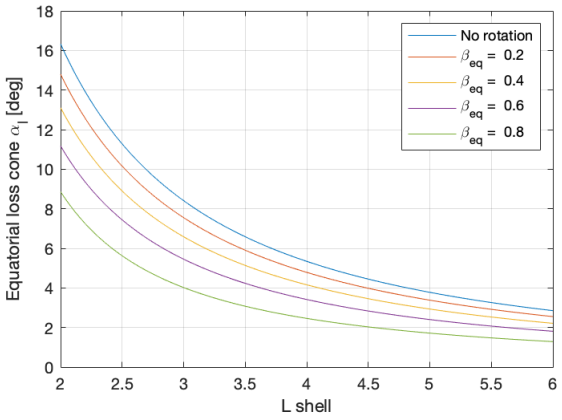

Figure 4.11: Equatorial loss cone α_l as a function of L shell values from L=2 to L=6, shown for when there is no rotation and when $\beta_{eq} = 0.2, 0.4, 0.6$ and 0.8.

5

Conclusion

5.1 Concluding remarks

In this study we wanted to investigate how the centrifugal force influences a trapped particle's bounce motion as described by the guiding centre approximation in a dipole magnetic field. We built on the existing model of Van Allen and Thomsen (1980) and included the effect of the centrifugal force. We assumed total energy and first adiabatic invariant to be conserved on the field line. From this, a model characterising a trapped particle's bounce motion in a rotating frame was derived (Chapter 3).

We first studied the particle's kinetic energy along the field in terms of the equatorial parameters E_{eq}, L and Ω_p, and how it affected the mirror point latitude λ_m. The particle dynamics was observed to be more affected by rotation if the particle was low energetic, is further out from the planet, or corotates with the angular frequency of a rapid rotating planet. Low energy particles bounce at lower latitudes as an effect of rotation, whereas high energy particles are almost not effected by rotation. Low energy particles that are further out from the planet will bounce at lower latitudes than those closer to the planet. Low energy particles corototating with a rapid rotating planet will bounce to lower latitudes compared to a non-rotating frame.

We then studied the the particle motion along the field line in terms of the β_{eq} parameter, which is the ratio of centrifugal potential energy to kinetic energy at equator. We found that particles are trapped closer to equator as an effect

of rotation, also for particles with small α_{eq} when β_{eq} is sufficiently large. The dimensionless function Φ was studied in terms of β_{eq} as well, and we observed Φ to behave differently depending on both β_{eq} and α_{eq}. Recalling the research question introduced in Section 1.1, we could in Chapter 3 and Chapter 4 discover that the combination of how mirror point latitude decreases, and inverse parallel velocity increases, resulted in varying values of Φ depending on the rate of change. The effect of rotation will therefore slow down particles along the field line and confine them towards equator, where β_{eq} is a prerequisite for the particle dynamics along the field line.

From the analysis in this study it is evident that conservation of energy and conservation of first adiabatic invariant put constraints on the particle motion along the field line. Compared to a non-rotating frame, a trapped particle's energy will behave as an oscillator along the field line as an effect of the rotating frame, converting between kinetic and potential energy. The total velocity of the particle along the guiding centre path is therefore constrained by conservation of energy. In addition, conservation of first adiabatic invariant will put a constrain on the perpendicular kinetic energy, as we know the magnetic field strength at every point along the field line. At which rate the particle energy converts between kinetic and potential energy, depends on the value of the β_{eq} parameter. From this it follows that at which rate parallel kinetic energy converts into perpendicular kinetic energy along the field line is determined by β_{eq} as well. The particle's total velocity is the sum of perpendicular and parallel velocity component squared, and explains why the particle motion along the field line is constrained by both conservation of energy and conservation of first adiabatic invariant. The bounce period of a trapped particle in a rotating frame is thus a two constrained problem determined by interplay between the two conservation laws.

5.2 Future work

A natural next step to improve the model presented in this thesis would be to investigate a particle's drift period in addition to the bounce period. The drift period introduced in Section 3.6 needs to be needs to be investigated in comparison to the bounce motion in order to obtain the complete dynamics of a trapped particle.

Another possible investigation could be to take into account how corotation of the magnetospheric plasma in the rotating system varies as a function of the radial distance in the magnetosphere as stated in Hill (1979).

We know it will take a few seconds for electrons to complete a bounce period. Since ions are heavier, they will spend a few minutes completing a bounce period. Based on this, it would also be interesting to investigate ions compared to electrons. The purpose of this would be to look at the bounce period difference of ions and electrons in a rotating frame, compared to a non-rotating frame. We would expect ions to spend longer time completing a bounce period than electrons due to their heaver mass.

Bibliography

N. Achilleos, P. Guio, and C. S. Arridge. A model of force balance in Saturn's magnetodisc. *MNRAS*, 401:2349–2371, February 2010. doi: 10.1111/j.1365-2966.2009.15865.x.

N. Achilleos, P. Guio, F. Hardy, C. Paranicas, and A. M. Sorba. The Magnetodisk Regions of Jupiter and Saturn. In R. Maggiolo, N. André, H. Hasegawa, D. T. Welling, and Paxton L. J. Zhang, Y. and, editors, *Magnetospheres in the Solar System*, chapter 29, pages 455–469. American Geophysical Union, 2021. doi: https://doi.org/10.1002/9781119815624.ch29.

W. Baumjohann and R. A. Treumann. *Basic Space Plasma Physics*. ICP, London, 1996. ISBN 1-86094-079-X.

Francis F. Chen. *Introduction to Plasma Physics and Controlled Fusion*. Springer Science+Business Media, New York, 1974. ISBN 978-1-4419-3201-3.

J. E. P. Connerney, M. H. Acuna, and N. F. Ness. Saturn's ring current and inner magnetosphere. *Nature*, 292:724–726, August 1981. doi: https://doi.org/10.1038/292724a0.

Gennaro D'Angelo and Jack J. Lissauer. Formation of giant planets. pages 1–25, 2018. doi: 10.1007/978-3-319-30648-3_140-1. URL `https://doi.org/10.1007/978-3-319-30648-3_140-1`.

P. Guio, N. Staniland, N. A. Achilleos, and C. S. Arridge. Trapped particle motion in magnetodisc fields. *JGR*, April 2020. doi: 10.1029/2020JA027827.

T. W. Hill. Inertial limit on Corotation. 84:6554–6558, November 1979. doi: 10.1029/JA084iA11p06554.

M. Kivelson and C. Russell. *Introduction to Space Physics*. Cambridge University Press, USA, 1st edition, 1995. ISBN 0-521-45104-3.

M. G. Kivelson. Planetary magnetodiscs: Some unanswered questions. *Space Science Reviews*, 187:5–21, 2014. doi: 10.1007/s11214-014-0046-6. URL `https://link.springer.com/content/pdf/10.1007/s11214-014-0046-6.pdf`.

M. G. Kivelson and F. Bagenal. Planetary Magnetospheres. In L.-A. A. McFadden, P. R. Weissman, and T. V. Johnson, editors, *AAS/Division for Extreme Solar Systems Abstracts*, pages 519–540. Elsevier, 2007. doi: 10.1016/B978-012088589-3/50032-3.

NASA. Explorer 1 overview, a. URL https://www.nasa.gov/mission_pages/explorer/explorer-overview.html.

NASA. Cassini at saturn, b. URL https://www.nasa.gov/mission_pages/cassini/main/index.html.

M. K. Öztürk. Trajectories of charged particles trapped in Earth's magnetic field. *American Journal of Physics*, 80:420–428, May 2012. doi: 10.1119/1.3684537.

PhysicsLibreTexts. Uniformly rotating frame. URL https://phys.libretexts.org/@go/page/30680.

Gerd. W. Prölss. *Physics of the Earth's Space Environment*. Germany, 2004. ISBN 3-540-21426-7.

Juan G. Roederer and Hui. Zhang. *Dynamics of Magnetically Trapped Particles*. Springer, Berlin, Heidelberg, 2nd edition, 2014. ISBN 978-3-642-41530-2.

D. G. Sibeck and K. R. Murphy. Large-Scale Structure and Dynamics of the Magnetosphere. In R. Maggiolo, N. André, H. Hasegawa, D. T. Welling, and Paxton L. J. Zhang, Y. and, editors, *Magnetospheres in the Solar System*, chapter 2, pages 15–36. American Geophysical Union, 2021. doi: https://doi.org/10.1002/9781119815624.ch2.

J. A. Van Allen and M. F. Thomsen. Motion of trapped electrons and protons in saturn's inner magnetopshere. *Journal of Geophysical Research*, 85:5831–5834, 1980. doi: 10.1029/JA085iA11p05831. URL https://agupubs.onlinelibrary.wiley.com/doi/abs/10.1029/JA085iA11p05831.

v. M. Vasyliunas. Comparing jupiter and saturn: dimensionless input rates from plasma sources within the magnetosphere. *Annales Geophysicae*, 26:1341–1343, 2008. doi: 10.5194/angeo-26-1341-2008. URL https://doi.org/10.5194/angeo-26-1341-2008.

M. F. Vogt, M. G. Kivelson, K. K. Khurana, R. J. Walker, Ashour-Abdalla, and E. J. Bounce. Simulating the effect of centrifugal forces in jupiter's magnetosphere. *Journal of Geophysical Research Space Physics*, 119:1925–1950, 2014. doi: 10.1002/2013JA019381.